國立臺灣大學理學院地質科學研究所

碩士論文

Department of Geosciences

College of Science

National Taiwan University

Master's Thesis

以電腦斷層掃描影像測量浮游性有孔蟲之形態特徵

Morphometric Characteristic of Planktonic Foraminifera using μ-Computed Tomographic data

陳威綸

Wei-Lun Chen

指導教授：羅立 博士

Advisor: Li Lo, PhD

中華民國 113 年 7 月

July, 2024

doi:10.6342/NTU202404142

國立臺灣大學碩士學位論文

口試委員會審定書

MASTER'S THESIS ACCEPTANCE CERTIFICATE
NATIONAL TAIWAN UNIVERSITY

以電腦斷層掃描影像測量浮游性有孔蟲之形態特徵

Morphometric characteristic of planktonic foraminifera using μ-computed tomographic data

本論文係陳威綸 (R11224112) 在國立臺灣大學地質科學系暨研究所完成之碩士學位論文，於民國 113 年 7 月 31 日承下列考試委員審查通過及口試及格，特此證明。

The undersigned, appointed by the Department of Geosciences, National Taiwan University on 31st July, 2023 have examined a Master's Thesis entitled above presented by Wei-Lun Chen (R11224112) candidate and hereby certify that it is worthy of acceptance.

口試委員 Oral examination committee:

（指導教授 Advisor）

系（所、學位學程）主管 Director: _____

doi:10.6342/NTU202404142

致謝

兩年的漫長歲月，終於把這個研究完成了，希望對於我未來的學術生涯是一個正向的開始，也終於不用每天靠香菸和魔爪強撐著趕論文，這個過程想想都要掉眼淚。這幾年的學術生涯中受到了很多人幫助，不管是研究理論、技術還是情感上，因此想在此表達我的感激之情。首先要謝謝大老闆羅立老師一路上的帶領，當年大學剛畢業的我有點茫然，大學時代跌跌撞撞碰壁無數的我對於自己有興趣的古生物領域懷抱了滿腔熱情，邁入研究所階段時卻找不太到比較適合自己的機會。是羅老師主動關心的訊息和提供的研究機會，讓我能找到具有強力未來潛力和發展性的研究計畫，尤其感謝老師給予的高自由度和空間，讓我可以彈性安排自己的時間和進度，不時的經驗分享和討論也使我更了解這個產業的方方面面，拓展我的眼界並有更多深度的思考。很抱歉每次寒暑假都直接消失一兩個月去當背包客、每次研討會都是臨時趕出來的投影片和當天印的海報、甚至最後半年才完成60%的工作，還好僥倖的產出了一些數據並在研究方法上有了點初步的發展，並騙了一篇期刊文章。非常期待未來有機會還能和老師與其他幾位相關實驗室成員的合作，個性上有些許稜角的地方非常抱歉，再煩請老師能多多包涵，我會認真成長的！

再來要謝謝擔任我口試委員的幾位老師：魏國彥老師、張永斌老師和簡至暐學長，在研究上提出了諸多的寶貴意見，讓我可以把論文修改到一個比較能看的品質。魏老師在有孔蟲型態研究和理論上的豐富經驗和犀利眼光，讓學生大為佩服，不曉得得花多少年的時間才能達到類似的學識狀態。另外張老師和簡學長也花了很多精力幫助修改論文錯誤並提供可能的修改方向，很大程度增進了我的寫作表達和論述能力，簡學長另外也協助我拍攝了不熟悉的 SEM 影像。感謝海研所的黃致展老師和師大地科系的葉孟宛老師提供 3D 的分析軟體，並且不厭其煩的在相關的操作上幫助我。感謝同步輻射中心的宋博、殷博和幾位學長姐在樣本掃描和影像重建上的幫助和指導，讓我可以在有限的時間內建立起用以分析的資料庫。感謝所有過去處理 ODP 1115B 相關研究的許多許多位學者，讓我有豐富的基礎資料可以運用，特別是智凱針對這根岩心的生物地層研究。

doi:10.6342/NTU202404142

研究室夥伴的部分，超級感謝 Rob 在同步中心做實驗的幫助和扶持，手拙的我每次都只能請他幫忙安放樣本到載台。很高興我們一起合力建立了一個稍具規模的有孔蟲影像資料庫，我絕不會忘記當年在同步一起做實驗一起跑重建程序的那些日與夜，另外英文寫作上的支援和研究上的諸多交流也讓我獲益良多，希望我的爛英文在未來還能有進步空間嗚嗚嗚。謝謝學弟鍶政幫忙準備口試的食物和飲料，還有立芃和易辰幫忙紀錄口委海量的問題和意見。感謝研究室助理鄭郁豫學姐和楊峻誌學長幫忙處理行政和教我畫圖，讓我可以減輕自己閉門造車的壓力。謝謝吳依璇學姊在最後的幾個月一直陪我聊天並安慰我、幫我檢查論文初稿的錯誤，衷心期許妳能早日通過資格考，獲得一些喘息的空間。

另外要謝謝很多好朋友的陪伴、幫助和鼓勵，高中同學邱育聖、石友周文博（方塊酥）、大學室友陳聿哲、生意夥伴彭良維、海大同學陳俊宇、高中學長宋冠毅、美國朋友 Jacky Li 和高中補習班老師熊。感謝這些朋友一直陪伴我、聽我吐苦水倒垃圾，並給我很多寶貴的人生建議。這是一篇不會有家人出現的致謝，但有好多在旅行上遇到的人都給了我相應的溫暖，支撐我走完這一路，永遠不會忘記把我撿回家住了一晚的塔吉克村長、尼泊爾村民，他們那麼貧窮，卻捨得把柴火和食物分給我，讓我在寒冷的冬夜能有個落腳之處。謝謝那些讓我搭便車的人，甚至還特地把我送回青旅門口。謝謝那些曾陪我一起旅行的各國夥伴，諸多的交流和分享讓我徹底喜歡上了在外面流浪。最後，當然也該謝謝吉爾吉斯坐地起價不成拿鐵鍬作勢砍我的黑車司機的不殺之恩和把我扣在新疆邊境審問四個小時卻沒有把我抓走的中國警察。

我要繼續當我的流浪漢去了，阿富汗見。

doi:10.6342/NTU202404142

Abstract

Globigerinoidesella fistulosa is an extinct planktonic foraminifera species occurred around 3.3-1.7 million years ago (Ma) in global tropical ocean. Its extinction event coincided and may be triggered by the formation and expansion of the modern Western Pacific Warm Pool (WPWP). Understanding its paleoecology would help testing the climate-induced hypothesis and further our knowledge to the climate-ecology interaction. So far, much uncertainty still exists about its ecological niche, such as biomass and photosymbiotic ecology. In this study, we performed 3D morphometric method to reconstruct the species' ecological niche, including volumetric and surface analysis using μ-CT reconstructions. Based on the previous studies on the ecology of modern *Trilobatus sacculifer*, a comparison between *G. fistulosa* and its relative *T. sacculifer* can be made here to better understand the former. The results of 3D analysis indicate larger biomass and surface area of *G. fistulosa* compared to *T. sacculifer*, which could be attributed to relatively abundant nutrient supply and enhanced symbiotic photosynthesis in the deeper part of the water column. Moreover, the surface area to total volume (S-V) ratio provides chance to inspect the variation of surface area through ontogeny of the two species. Compared to *T. sacculifer*, *G. fistulosa* generally registers higher S-V ratio under similar body size, as well as higher variation. For *G. fistulosa*, the higher surface area per total volume (might resulted from the flat, irregular gross morphology and protuberance. More theoretical studies would be required to confirm the hypothesis) might bring about a larger potential for spines across the surface space. The morphological traits would likely counteract the settling force provided by the hypothesized increase in shell test and overall density. Our interpretations toward the ecology of *G. fistulosa* is based on the previous study of shell geochemistry, as it implies the calcification depth of *G. fistulosa* might been deeper in depth than its ancestor *T. sacculifer* based on the Mg/Ca ratio and $\delta^{18}O$ data.

Key words: Planktonic foraminifera, early Pleistocene, ecology, morphometrics, μ-CT, the Western Pacific Warm Pool

doi:10.6342/NTU202404142

中文摘要

Globigerinoidesella fistulosa 是一已滅絕的熱帶浮游性有孔蟲物種，大約在 330 萬到 170 萬年前生存於全球熱帶海域。其滅絕事件與現代西太平洋暖池（WPWP）的形成和初步擴張之發生時間重合且可能有潛在的連結。了解其古生態學有助於檢驗氣候誘導的假說，並進一步增進我們對古氣候與生物圈間相互作用的認識。迄今為止，該物種的生態位仍存在許多不確定性，如其生物量與光合共生藻之互動關係。在本研究中，我們採用了三維形態計量方法嘗試重建了該物種的生態位，包括使用 μ-CT 重建進行體積和表面分析。基於前人研究對其祖先和親緣物種 *Trilobatus sacculifer* plexus 之生態特性已有較多的著墨，我們將 *G. fistulosa* 和其親緣物種 *T. sacculifer* plexus 進行比較，以更好地理解前者。3D 立體型態分析結果表明，*G. fistulosa* 的生物量和殼體表面積較 *T. sacculifer* plexus 更大，這可能歸因於混合層較深處相對豐富的營養供應，並因此形成較強的共生光合作用。此外，表面積與總體積（S-V）之比值提供了檢驗兩種物種在個體發育過程中的表面積變化的機會。與 *T. sacculifer* plexus 相比，*G. fistulosa* 通常在相似的體型下具有較高的 S-V 比值，且不同個體間的 S-V 比值差異也更大。對於 *G. fistulosa*，較高的 S-V 比值（可能是由於較扁平、不規則的殼體型態和指狀突起所致，此假設需要更多理論研究確認）增加了殼體表面容納更多刺的空間。此型態特徵可能會抵消在假設上殼體較高的殼體密度和總密度所帶來的沉降力。我們對 *G. fistulosa* 生態學的解釋基於先前對其殼體地球化學的研究，其表明根據 Mg/Ca 比率和 $\delta^{18}O$ 數據，*G. fistulosa* 的造殼深度可能比其祖先 *T. sacculifer* plexus 更深。

doi:10.6342/NTU202404142

Contents

doi:10.6342/NTU202404142

doi:10.6342/NTU202404142

doi:10.6342/NTU202404142

doi:10.6342/NTU202404142

Figures

doi:10.6342/NTU202404142

doi:10.6342/NTU202404142

doi:10.6342/NTU202404142

Tables

doi:10.6342/NTU202404142

Chapter 1: Introduction

The extinct planktonic foraminifera species *Globigerinodesella fistulosa* (Schubert, 1910), as the descendent of *Trilobatus sacculifer* plexus, occurred in global tropical ocean around 3.3-1.7 million years ago (Ma). Its last appearance datum (LAD) is widely used as an age index for defining the biozone PT1a (~the boundary of Gelasian and Calabrian) for tropical marine core (Wade et al., 2011). Interestingly, the extinct timing of *G. fistulosa* is somehow coincided with the formation and initial expansion of the Western Pacific Warm Pool (WPWP) (Wara et al., 2005), implying the environmental change as a possible evolutionary driver for the organism. Therefore, the ecological niche and the associated functional morphology of *G. fistulosa* would be the first priority to be pinpointed. However, apart from the systematic paleontology (Poole and Wade, 2019; Spezzaferri et al., 2015) and the datum event (Chuang et al., 2018; Wade et al., 2011), our current knowledge upon the species including morphological variation, functional morphology and paleoecology is quite limited. As the descendent of *T. sacculifer* plexus, *G. fistulosa* often compared and studied with its ancestor. The previous studies of *T. sacculifer* covering morphology, laboratory culture, ecology and biostratigraphy (Brummer et al., 1987; Hemleben et al., 1987) (Bé, 1980; Bijma et al., 1990; Chuang et al., 2018; Poole and Wade, 2019; Wade et al., 2011) provide possibility to further our knowledges toward *G. fistulosa* through morphometric and geochemical comparison. Under morphology-based systematic framework, four morphospecies are covered for *T. sacculifer* plexus based on coiling and the morphology of the ultimate chamber: *T. trilobus*, *T. immaturus*, *T. quadrilobatus* and *T. sacculifer* sensu stricto (Brady, 1877; d'Orbigny, 1846; LeRoy, 1939; Reuss, 1850). Nonetheless, these morphospecies are revealed as the same biological species (Bé, 1980) under laboratory

doi:10.6342/NTU202404142

culturing (except *T. immaturus*, which was not observed in the culturing result). Alternatively, another morphological framework related to ontogeny and laboratory ecological treatments was introduced based on the morphology of the last chamber (NOR/Normal and SAC forms with globular or sac-like ultimate chamber) and the smaller or equal size of ultimate chamber in comparison with the penultimate chamber (KUM/Kummer form, first proposed by Berger (1969)) (Brummer et al., 1987; Hemleben et al., 1987). The NOR/Normal form usually refers to the pre-gametogenic phases, while the SAC form represents the individuals with impending gametogenesis, along with spine-shedding (Bé, 1980). The kummer form is found not only on T. sacculifer, but also other species (Bijma et al., 1990; Olsson, 1972). The reason causes the reach of growth limit is still unknown, but more likely attributed to genetic control rather than environmental stress (Olsson, 1973). In laboratory culturing experiments, no tendency of any environmental stresstor were observed (Bijma et al., 1990; Bijma and Hemleben, 1994; Brummer et al., 1987).

Chen (2006) studied the size distribution of *G. fistulosa* (or Fis form in her study) and *T. sacculifer* plexus under the sieving size framework and Normal/Kummer/Sac-like framework. The result shows *G. fistulosa* is generally larger than *T. sacculifer* plexus in size. However, the size fraction method only records the width of the organisms as the size index and without includes the information of length and chamber morphology. With insufficiency of critical information, the misestimation of the size difference and biomass of the two species would be inevitable. Chen (2008) examined the shell chemistry of *G. fistulosa* by comparing it with its ancestor stock, *T. sacculifer* plexus. The result shows strong trophic dependency (symbiotic $\delta^{13}C$ fractionation) and deeper habitats for the species (heavier $\delta^{18}O$

doi:10.6342/NTU202404142

values and lower Mg/Ca ratio) for *G. fistulosa*. However, the use of gross shell, nevertheless, brings about the observational bias as the result of geochemical analysis is highly susceptible to the size and calcification process of the last chamber (which supposed to be larger in size and formed in deeper water depth). More advanced understanding towards ecology would be critical for interpreting the shell geochemistry in details, especially cross-sectional geochemical mapping (Hori et al., 2018). Exponential relationship between maximum test size and test surface area based on 2D photography is found for *G. fistulosa* and *T. sacculifer* plexus (Poole and Wade, 2019). The 2D photography could be linked to some differences found between the two species, as the right-shift characteristic is found upon the data. Therefore, in order to further our understanding toward the morphological variation and ecology of *G. fistulosa*, a more comprehensive morphological analysis throughout the body of foraminifera would be requisite.

The study of foraminifera against its morphology has been highly rely on 2D photography and sieving size for decades (Depuydt et al., 2023; Olsson, 1972; Spezzaferri et al., 2015; Wei, 1987). The 2D photography remains limited under the restrictions of optical microscopes and related image processing procedures, as the 3D geometric information behind the complicated test morphology is often ignored, leading to biases into systematic and analytical studies. Some morphological characteristics that critical for ecological studies, such as total volume, chamber cumulative volume, would never be feasible under 2D aspects. The sieving techniques provide first ordered size measurement to the studied materials. Nevertheless, estimation of biomass and ontogenetic growth would meet difficulties and can never be accurate. Furthermore, to explore the complicated 3D test geometry and internal structures of foraminifera, invasive protocols such as serial dissection are widely applied

doi:10.6342/NTU202404142

under time-consuming problem and predominantly rely on the expertise of the researchers (Görög et al., 2012). Despite the non-invasive scanning electron microscope (SEM) was introduced in 1960s (Hay and Sandberg, 1967), its disadvantage attributed to sample preparation procedures such as Au/C coating and holder fixation would stop the reuse of samples for further studies (Görög et al., 2012).

The recent innovation of CT technology and 3D analysis software offers new insight into the morphological study of foraminifera, allowing measurements such as chamber volume, surface area (Belanger, 2022; Burke et al., 2020; Caromel et al., 2016; Vanadzina and Schmidt, 2022) and geometric chamber growth (Brombacher et al., 2022) become more feasible and reliable. The internal structure of the test can easily be observed and measured, e.g., the of early developed chamber (such as proloculus and the subsequent 10 chambers) (Duan et al., 2021), Moreover, the measurement of shell density through calculation of CT numbers (Iwasaki et al., 2019) or the total surface area per unit (Signes et al., 1993) of volume provide efficient and accurate solutions. Critically, the non-invasive and therefore non-destructive features of CT scan allowing the scanned sample can still be available for further reassessment, as duplication, archiving and long-term storage of digital 3D CT image provide perpetual accessibility to the data.

Here we present a study regarding the 3D analysis of morphological variation and ecological assessment toward the planktonic foraminifera species *G. fistulosa* by comparing with its ancestor stock *Trilobatus sacculifer* plexus. Three morphological forms are assigned to the studied materials: Fis form (*G. fistulosa*), the Normal and the Sac-like form (*Trilobatus sacculifer* plexus, prior and in gametogenic phase). Through the reconstruction of total

doi:10.6342/NTU202404142

volume (including calcareous skeleton and chamber cavity), surface area and surface area to total volume ratio (S-V ratio) with the CT analysis software *ORS Dragonfly* and a combined discussion with the previous researches, the knowledges toward biomass, symbiotic photosynthesis, adaptive functional morphology and trophic mode of *G. fistulosa* (Fis form) are improved. To assess the ENSO-like environment before the extinction of *G. fistulosa* (Fis form) (around 1.7 Ma), the bathymetric profiles of nutrients and salinity are produced for modern ocean condition (Normal condition in the Solomon sea) with the software *Ocean Data View* (Schlitzer, 2023). The presented data is then discussed combined with the vertical structure reconstructed in Chen (2008) for the Solomon sea (1.767-1.713.).

doi:10.6342/NTU202404142

Chapter 2: Materials and Methods

2.1 Studied materials

A total of 166 fossil planktonic foraminifera individuals of *G. fistulosa* (Fis form) and its ancestor stock *T. sacculifer* plexus (which divided into Normal and Sac-like forms in this study) specimens across 9 horizons (1.765, 1.764, 1.763, 1.758, 1.748, 1.745, 1.742, 1.729, 1.720 Ma) from ODP Hole 1115B (Solomon Sea, the South Pacific Ocean) prior to and after the extinction event of *G. fistulosa* (Fis form) are examined, with size fractions in between 250-300, 300-355, 355-425, 425-500, 500-600 and larger than 600 μm. For *G. fistulosa*, the specimens from all size fractions are included. While for Normal and Sac-like forms of *T. sacculifer* plexus, samples in between 250-300, 300-355, 355-425, 425-500, 500-600, larger than 600 μm and 250-300, 355-425, 425-500, 500-600 and larger than 600 μm are included.

As for horizons, the *G. fistulosa* (Fis form) specimens cover 6 horizons (1.765, 1.764, 1.763, 1.758, 1.748, 1.745 Ma). As Normal and Sac-like forms, 5 horizons (1.763, 1.758, 1.748, 1.742, 1.720 Ma) and 6 horizons (1.763, 1.758, 1.748, 1.742, 1.729, 1.720 Ma) are covered, respectively. All the specimens were obtained through processes such as hand-washing, sieving and hand-picking under optical microscope.

Some intermediate forms of *G. fistulosa* and *T. sacculifer* with incipient protuberance (s) are found in the samples. According to the previous perspectives, in order to keep the biostratigraphic significance of *G. fistulosa*, the intermediate forms are rather viewed as extreme phenotypes of *T. sacculifer* (Poole and Wade, 2019). These samples are not included in this study as the aim is to include only the standard morphology of every firm.

doi:10.6342/NTU202404142

Besides, another rule is applied on *T. sacculifer* plxus samples to differentiate different morphologies. Two forms, Normal form (e.g., *T. trilobus*, *T. quadrilobatus* and *T. immaturus*) and Sac-like form (*T. sacculifer* sensu stricto) are defined here for the individuals with and without sac-like last chamber. The Kummer form which included in the previous researches is not covered in this study due to unclear reason that cause the growth limits (Olsson, 1973).

To avoid inadequacy of available *G. fistulosa* (Fis form) specimens, all the samples with one broken protuberance are included in this study.

doi:10.6342/NTU202404142

Table 2.1 List of the foraminifera samples used for 3D morphological analysis.

Morphotypes	Species	Hole	Age horizons	Size fractions	Numbers
Normal form	*T. sacculifer*	ODP 1115B	1.763 Ma, 1.758 Ma 1.748 Ma, 1.742 Ma, 1.720 Ma	250-300 μm 300-355 μm, 355-425 μm, 425-500 μm, 500-600 μm, >600 μm	61
Sac-like form	*T. sacculifer*	ODP 1115B	1.763 Ma, 1.758 Ma, 1.748 Ma, 1.742 Ma, 1.729 Ma 1.720 Ma	250-300 μm 355-425 μm 425-500 μm, 500-600 μm, >600 μm	41
Fis form	*G. fistulosa*	ODP 1115B	1.765 Ma, 1.764 Ma, 1.758 Ma, 1.748 Ma, 1.745 Ma	250-300 μm, 300-355 μm, 355-425 μm, 425-500 μm, 500-600 μm, >600 μm	53

doi:10.6342/NTU202404142

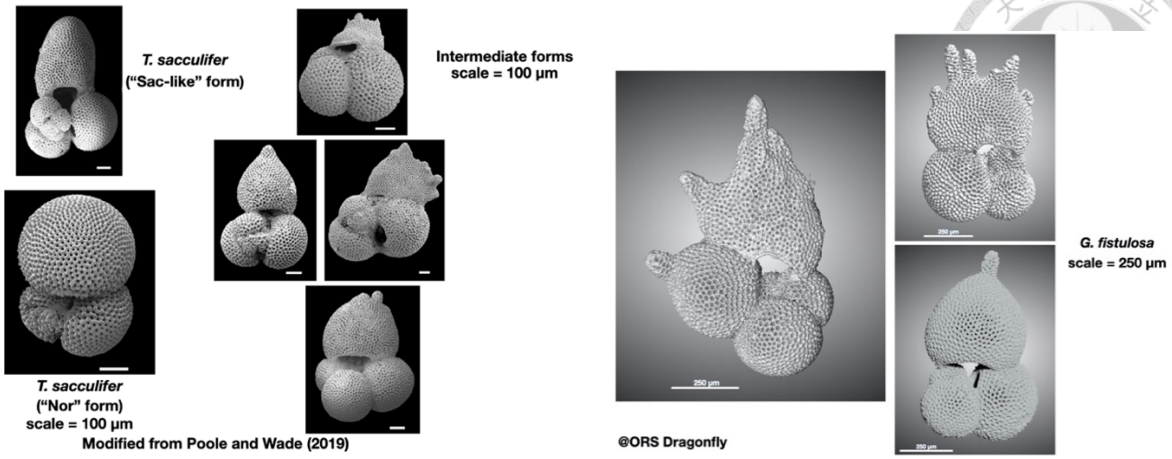

Figure 2.1 Morphological framework of this study. The studied materials are divided into three forms: the Fis (*G. fistulosa*), Normal (*T. sacculifer* with rounded last chamber) and Sac-like form (*T. sacculifer* with sac-last chamber). To be noted, the intermediate forms with protuberance-bearing chamber (s) are considered as Fis form in this study.

2.2 ODP Hole 1115B

ODP Hole 1115B is located in the Woodlark rise, the Solomon Sea, southwestern Pacific Ocean (9°11'S, 151°34'E, 1149 m water depth) (Figure 2.2), which is one of the three holes drilled in ODP Site 1115. The hole is 293.1 m in total length, with 286.84 m recovered (98%). In the lithostratigraphic unit II (35.7–149.7 meter below sea floor, mbsf) within the core, the lithologies are mainly composed of ooze and clay. For volcanic ash, numerous layers of epiclastic origin are present (Chuang et al., 2018; Taylor et al., 1999). All the samples used in this study are from the lithostratigraphic unit II and preserved in perfect condition (with no seawater corrosion and diagenesis-free), with the stratigraphic interval in between 10H5W (1.764 Ma) to 10H2W (1.720 Ma).

doi:10.6342/NTU202404142

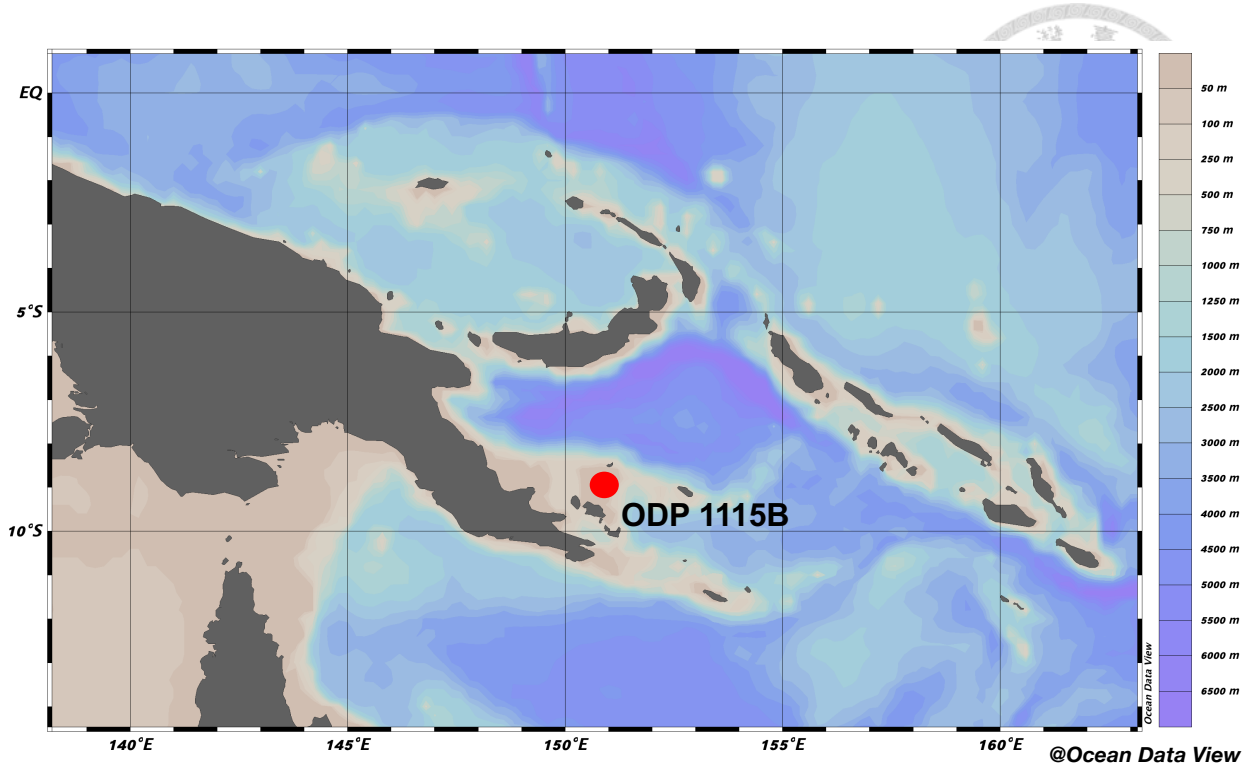

Figure 2.2 Bathymetric map of ODP Hole 1115B. The map shows the location of the drilling site in the Solomon Sea, the Western Pacific Ocean. The map is produced by the software *Ocean Data View* (Schlitzer, 2023).

2.3 Age model

The age model of ODP Hole 1115B applied here is based on Chuang et. al. (2018). The age model was established based on biostratigraphy (calcareous nannofossils event and planktonic foraminiferal datum event) and magnetic reversals with a correlation of the *Trilobatus sacculifer* $\delta^{18}O$ record (300–355 μm) to a global LR04 stack (Lisiecki and Raymo, 2005). The average sedimentation rate is ~7 cm/kyr (Takahashi et al., 2001). Figure 2.3

doi:10.6342/NTU202404142

shows the age-depth relationship of ODP Hole 1115B based on paleomagnetism, biostratigraphy and radioactive dating methods.

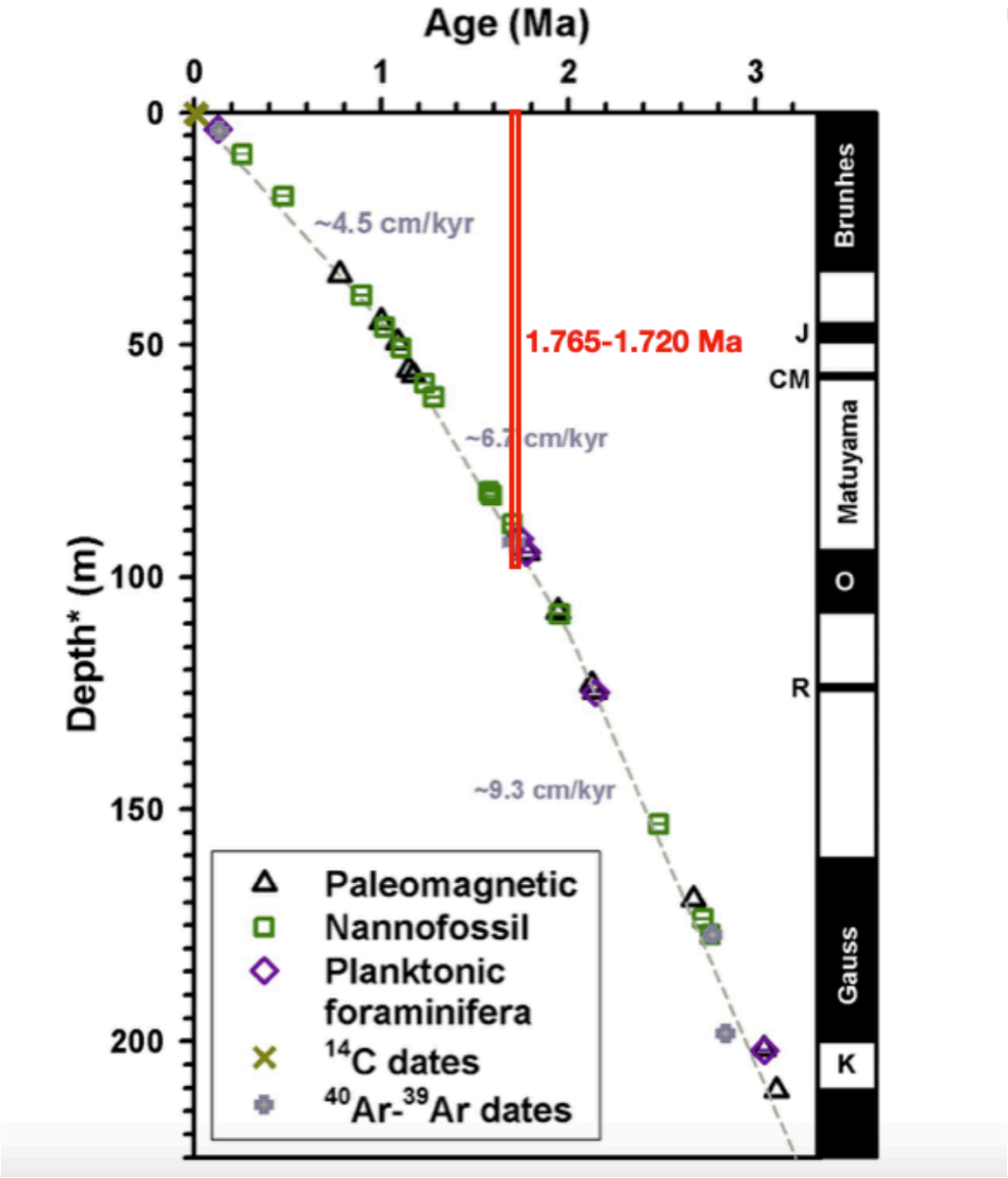

Figure 2.3 Age-depth plot of ODP Hole 1115B. It is based on paleomagnetism (black triangle), calcareous nannofossil events (green square), planktonic foraminiferal datum

doi:10.6342/NTU202404142

events (purple diamond), planktonic foraminiferal AMS ^{14}C (yellow cross), and volcanic glass ^{40}Ar-^{39}Ar dates (gray cross). The Paleomagnetic epochs are combined at the right side. The age interval where the samples used is remarked on it (1.765-1.720 Ma). The figure is revised from Chuang et. al. (2018).

2.4 μ-CT reconstruction and protocols of projection X-ray microscopy

Three-dimensional μ-CT reconstructions for the fossil samples were generated with projection X-ray microscopy (PXM) system at beamline TPS31A of the Taiwan Photon Source at National Synchrotron Radiation Research Center (NSRRC) in Hsinchu, Taiwan. Each scan was carried on one sample only. The X-ray energy adopted for scanning is ranging from 22-30 keV。The field of view of image is 8 × 2 mm^2. Tomography was implemented by performing azimuthal rotations at intervals of 0.25 degrees over the full range of ±90 degrees, resulting in a total of 721 projection images. With filtered-back-projection reconstruction algorithm, the CT reconstruction were eventually produced. With 10× objective lens and bin 2 algorithm, the spatial resolution of the preliminary 2D image is 2.6 μm and the pixel size is 1.3 μm. The standard deviation (%) of width, height, thickness, and absorption of one sample in 20 analysis is 0.09%, 0.18%, 0.01%, and 2.9%, respectively. The advanced details can be found in Chen et al. (2023).

Before the scanning process, each sample was placed on a wax or plastic holder. One tray can hold 40 samples. The x-y-z coordinate of each sample with holder on tray was manually measured by an image measurement instrument and recorded. Then, the tray was put in the end-station and the projection images were processed automatically by using a robot for putting each sample to the sample holder of the experimental stage. The temporal

doi:10.6342/NTU202404142

resolution of one tomography is about 1−2 minutes according to the exposure time of the image. After the projection image scanning procedure, the computed reconstruction process was followed behind to convert the 2D image set of each foraminifer into 3D reconstruction. The reconstruction is always conducted with bin 2 algorithm, while bin 1 algorithm is also available for higher resolution. Finally, a 3D raw file is produced for each foraminifer sample (Figure 2.4).

2.5 3D morphometrics

The 3D morphometric analysis is carried out on the 3D reconstruction images using *ORS Dragonfly* (Version 2022.2**)** software and *Bone analysis* plugin. The raw files were first input into the software, with the length of x, y, z axes being set manually.

A watertight model is first generated for each 3D image for total volume and surface calculation in *Bone analysis* plugin. To create the watertight model, the calcific skeleton of foraminifera was first segregated from the raw file as an ROI (region of interest) using Otsu binary segmentation. To make the ROI clean with no noise spots and tiny fossil fragments left, cleaning process is taken manually with brush tool to erase those unwanted by putting a low value in the hole-filling step (it can be either 0 or1-3 μm). After it, an ROI with only the skeleton left is created. The cavity of the skeleton ROI was then filled in the plugin with the bone filling step (by inputting a value that is larger than the aperture, usually 60-80 μm). For G. fistulosa (Fis form), the space in betweenthe protuberances is usually filled by the program and required further removing the ROI manually. Afterall, a mesh is created for both total

doi:10.6342/NTU202404142

volume and surface calculation, with the value of surface area-total volume ratio can then be computed on the software *Excel*. The idea of watertight model generation is inspired by Burke et al. (2020)

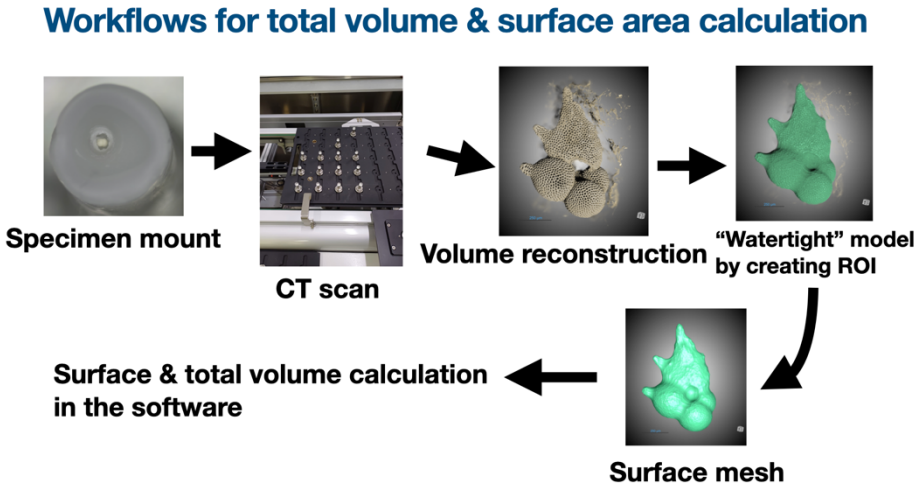

Figure 2.4 Workflows for 3D total volume and surface area calculation in this study. The steps including mounting samples on the standing for CT scan, 3D volume reconstruction, creating watertight ROI in the plugin *Bone analysis* in the software *Dragonfly*, converting the ROI into surface mesh file and the data calculation in *ORS Dragonfly*.

2.6 Descriptive statistics, Box plot and histogram

A table of descriptive statistics of total volume, surface and surface-total volume ratio for each foraminifera form are generated by using data analysis function in software *Excel*. The statistical parameters covered are: Mean, Standard Error, Median, Standard Deviation, Sample Variation, Kurtosis, Skewness, Range, Minimum, Maximum, Sum and Sample numbers. Besides, boxplot and histogram are drawn using software *OriginPro* 2021 (OriginLab Corporation, Version 2021).

doi:10.6342/NTU202404142

2.7 Two-sample student t-test

The two-sample t-test is carried with the software *PAST* 4.03 (Hammer and Harper, 2001) to see if the samples are significantly different to each other. The three forms are compared one to one as Fis vs. Normal, Fis vs. Sac-like, Normal vs. Sac-like forms, respectively. To see if there's a difference in between each two forms, the p-values of the forms are calculated and compared in both equivalent/inequivalent variance.

2.8 Bathymetric profile of nutrients and salinity

The bathymetric profile of nutrients (nitrate and phosphorate) and salinity of the Solomon Sea are generated by using dataset WOA 2005 (World Ocean Atlas 2005) released by National Centers for Environmental Information, National Oceanic and Atmospheric administration (NOAA). WOA 2005) is a dataset of objectively analyzed (1° grid) climatological fields of in situ globally scaled marine envieonmental factors such as temperature, salinity, and nutrients at standard depth levels for certain period of time scale such as annual, seasonal, and monthly. In addition, observed oceanographic profile data is also included in the dataset. The raw data includes data from 1995 to 2005 is averaged and imported into the software *Ocean Data View* for the depth profile visualization of modern ocean condition in the Solomon Sea (an area approximately in between 6°S-14°S and 150°E-160°E is applied). The scale from 0-500 m is applied on the figures of the three environmental stressors. The figures of the bathymetric profile can be found in Appendix 3.1-3.3.

doi:10.6342/NTU202404142

Chapter 3: Results

3.1 Total volume

3.1.1 Distribution of *G. fistulosa* (Fis form)

Totally 53 *G. fistulosa* (Fis form) specimens are included. The data are plotted along with *T. sacculifer* (Normal and Sac-like forms) in the boxplot (Figure 3.1) and the histogram (Figure 3.2) to show the total volume distribution, with the partial result of descriptive statistics summarized in table 3-1. The value of total volume data is ranging from 3.04×10^7 μm^3 to 1.96×10^8 μm^3, with mean at 9.95×10^7 μm^3 and standard deviation at 4.18×10^7 μm^3.

3.1.2 Distribution of *T. sacculifer* (Normal form)

Totally 64 *T. sacculifer* (Normal form) specimens are included. The data are plotted in the boxplot (Figure 3.1) and the histogram (Figure 3.2) to show the total volume distribution, with the descriptive statistics summarized in table 3-1. The value of total volume data is ranging from 1.16×10^7 μm^3 to 8.16×10^7 μm^3, with mean at 4.29×10^7 μm^3 and standard deviation at 2.19×10^7 μm^3.

3.1.3 Distribution of *T. sacculifer* (Sac-like form)

Totally 41 *T. sacculifer* (Sac-like form) specimens are included. The data are plotted in the boxplot (Figure 3.1) and the histogram (Figure 3.2) to show the total volume distribution, with the descriptive statistics summarized in table 3-1. The value of total volume data is ranging from 1.42×10^7 μm^3 to 1.12×10^8 μm^3, with mean at 4.73×10^7 μm^3 and standard deviation at 2.63×10^7 μm^3.

doi:10.6342/NTU202404142

3.1.4 Comparison between *G. fistulosa* (Fis form) and *T. sacculifer* (Normal and Sac-like forms)

The total volume comparison in between Fis vs. Normal, Fis vs. Sac-like and Normal vs. Sac-like forms are made with mean value and Two-sample student t-test. By the comparing the mean value, in the Fis vs. Normal group, the mean value in Fis is higher than Normal, about 121.3%. In the Fis vs. Sac-like group, the mean value in Fis is higher than Sac-like, about 100.7%. In the Normal vs. Sac-like group, Sac-like form is 10.3% larger than Normal form. As for the result of the Two-sample student t-test, Fis form shows significant difference to both Normal and Sac-like forms. As for the comparison of Normal vs. Sac-like forms, the result shows no significant difference in between the two. The detailed step-by-step result of the t-test is attached in Appendix 1.1-1.3 and the complete descriptive statistics is attached in Appendix 2.1.

Table 3.1 Descriptive statistical comparison of the total volume of Fis, Normal and Sac-like forms.

	G. fistulosa **(Fis form)**	***T. sacculifer*** **(Normal form)**	***T. sacculifer*** **(Sac-like form)**
Mean	9.95×10^7 μm³	4.29×10^7 μm³	4.73×10^7 μm³
Standard deviation	4.04×10^7 μm³	2.19×10^7 μm³	2.63×10^7 μm³
Minimum	3.04×10^7 μm³	1.16×10^7 μm³	1.42×10^7 μm³
Maximum	1.96×10^8 μm³	8.16×10^7 μm³	1.12×10^8 μm³
Sample numbers	53	61	41

doi:10.6342/NTU202404142

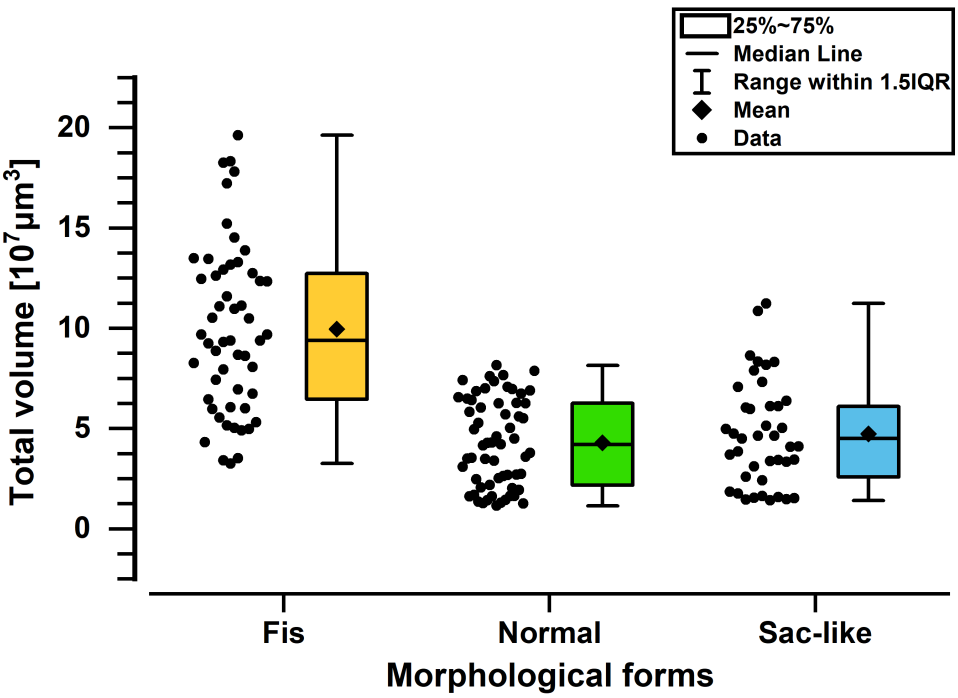

Figure 3.1 Boxplot for the total volume distribution of Fis (the orange box in the left), Normal (the green box in the middle) and Sac-like (the blue box in the right) forms. Each form is presents with the box of 25th-75th percentile, median line, range within 1.5IQR (range in between maximum and minimum values), mean point (filled diamond) and data point (filled circle). Based on the result of student t-test, Fis form is showing predominantly different distribution compare to the others, while Normal and Sac-like forms are showing no significant difference from each other.

doi:10.6342/NTU202404142

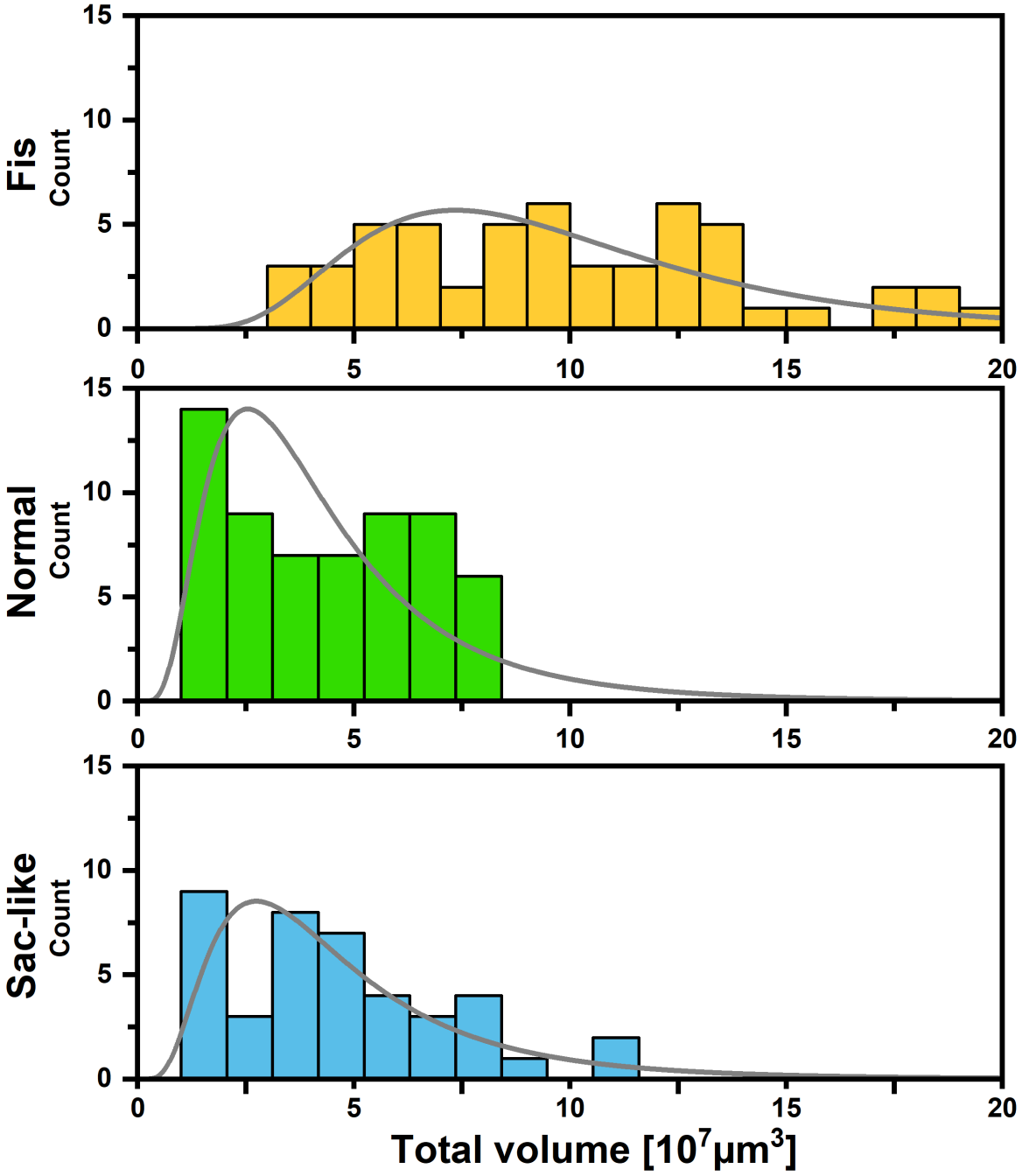

doi:10.6342/NTU202404142

Figure 3.2 Histogram and line graph for the total volume distribution of Fis (orange histogram in the top), Normal (green histogram in the middle) and Sac-like (blue histogram in the bottom) forms. It shows the variation of sample distribution across Fis, Normal and Sac-like forms.

3.2 Surface area

3.2.1 Distribution of *G. fistulosa* (Fis form)

Totally 53 *G. fistulosa* (Fis form) specimens are included. The data are plotted in the boxplot (Figure 3.3) and the histogram (Figure 3.4) to show the surface area distribution, with the descriptive statistics summarized in table 3.2. The value of surface area data is ranging from 6.12×10^5 μm² to 2.85×10^6 μm², with mean at 1.45×10^6 μm² and standard deviation at 4.87×10^6 μm². To be noted, an outlier is found at 2.85×10^6 μm².

3.2.2 Distribution of *T. sacculifer* (Normal form)

Totally 61 *T. sacculifer* (Normal form) specimens are included. The data are plotted in the boxplot (Figure 3.3) and the histogram (Figure 3.4) to show the surface area distribution, with the descriptive statistics summarized in table 3.2. The value of surface area data is ranging from 2.82×10^5 μm² to 1.097×10^6 μm², with mean at 6.91×10^5 μm² and standard deviation at 2.62×10^5 μm².

3.2.3 Distribution of *T. sacculifer* (Sac-like form)

Totally 41 *T. sacculifer* (Sac-like form) specimens are included. The data are plotted in the boxplot (Figure 3.3) and the histogram (Figure 3.4) to show the surface area

doi:10.6342/NTU202404142

distribution, with the descriptive statistics summarized in table 3.2. The value of surface area data is ranging from 3.33×10^5 μm ^{2} to 1.46×10^6 μm^2, with mean at 7.54×10^5 μm^2 and standard deviation at 3.07×10^5 μm^2.

3.2.4 Comparison between *G. fistulosa* and *T. sacculifer* (Fis, Normal and Sac-like forms)

The surface area comparison in between Fis vs. Normal, Fis vs. Sac-like and Normal vs. Sac-like forms are made with mean value and Two-sample student t-test. By comparing the mean value, in the Fis vs. Normal group, the mean value in Fis is higher than Normal, about 102.6 %. In the Fis vs. Sac-like group, the mean value in Fis is higher than Sac-like, about 85 %. In the Normal vs. Sac-like forms, Sac-like form is 9.14% higher than the Normal form. As for the result of the Two-sample student t-test, Fis form shows significant difference to both Normal and Sac-like forms. As for the comparison of Normal vs. Sac-like forms, the result shows no significant difference in between the two. The detailed result of the t-test is attached in Appendix 1.4-1.6 and the complete descriptive statistics is attached in Appendix 2.2.

doi:10.6342/NTU202404142

Table 3.2 Descriptive statistical comparison of the surface area of Fis, Normal and Sac-like forms.

	G. fistulosa **(Fis form)**	***T. sacculifer*** **(Normal form)**	***T. sacculifer*** **(Sac-like form)**
Mean	1.45×10^6 μm²	6.91×10^5 μm²	7.54×10^5 μm²
Standard deviation	4.87×10^6 μm²	2.62×10^5 μm²	3.07×10^5 μm²
Minimum	6.12×10^5 μm²	2.82×10^5 μm²	3.33×10^5 μm²
Maximum	2.85×10^6 μm²	1.097×10^6 μm²	1.46×10^6 μm²
Sample numbers	53	61	41

doi:10.6342/NTU202404142

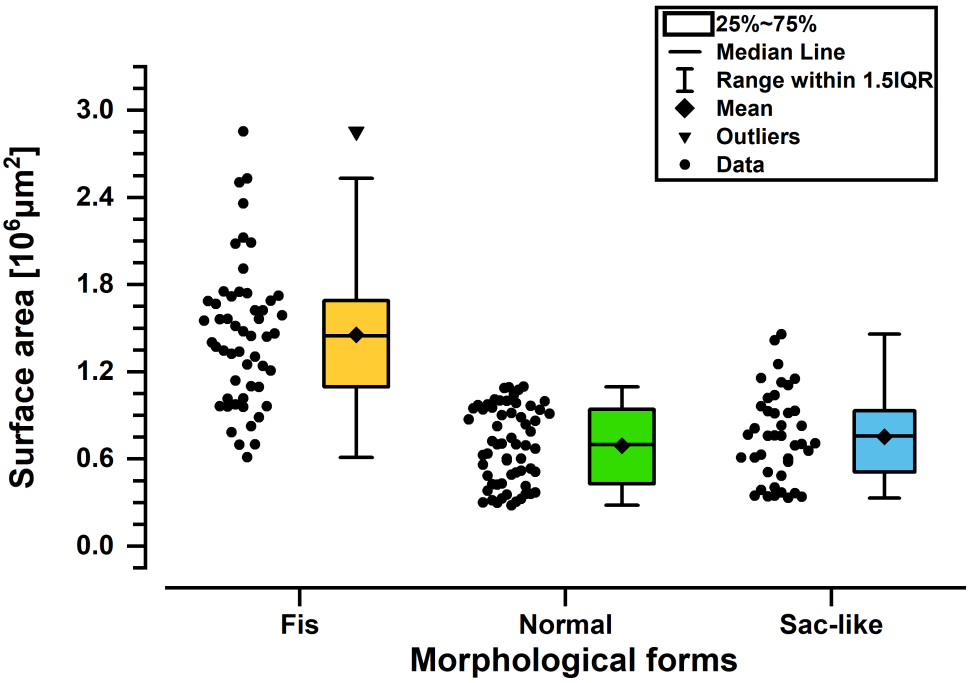

Figure 3.3 Boxplot for the surface area distribution of Fis (the orange box in the left), Normal (green box in the middle) and Sac-like (blue box in the right) forms. Each form is presents with the box of 25th-75th percentile, median line, range within 1.5IQR (range in between maximum and minimum values), mean point (filled diamond) and data point (filled circle). Based on the result of student t-test, Fis form is showing predominantly different from the others, while Normal and Sac-like forms are showing no significant difference from each other.

doi:10.6342/NTU202404142

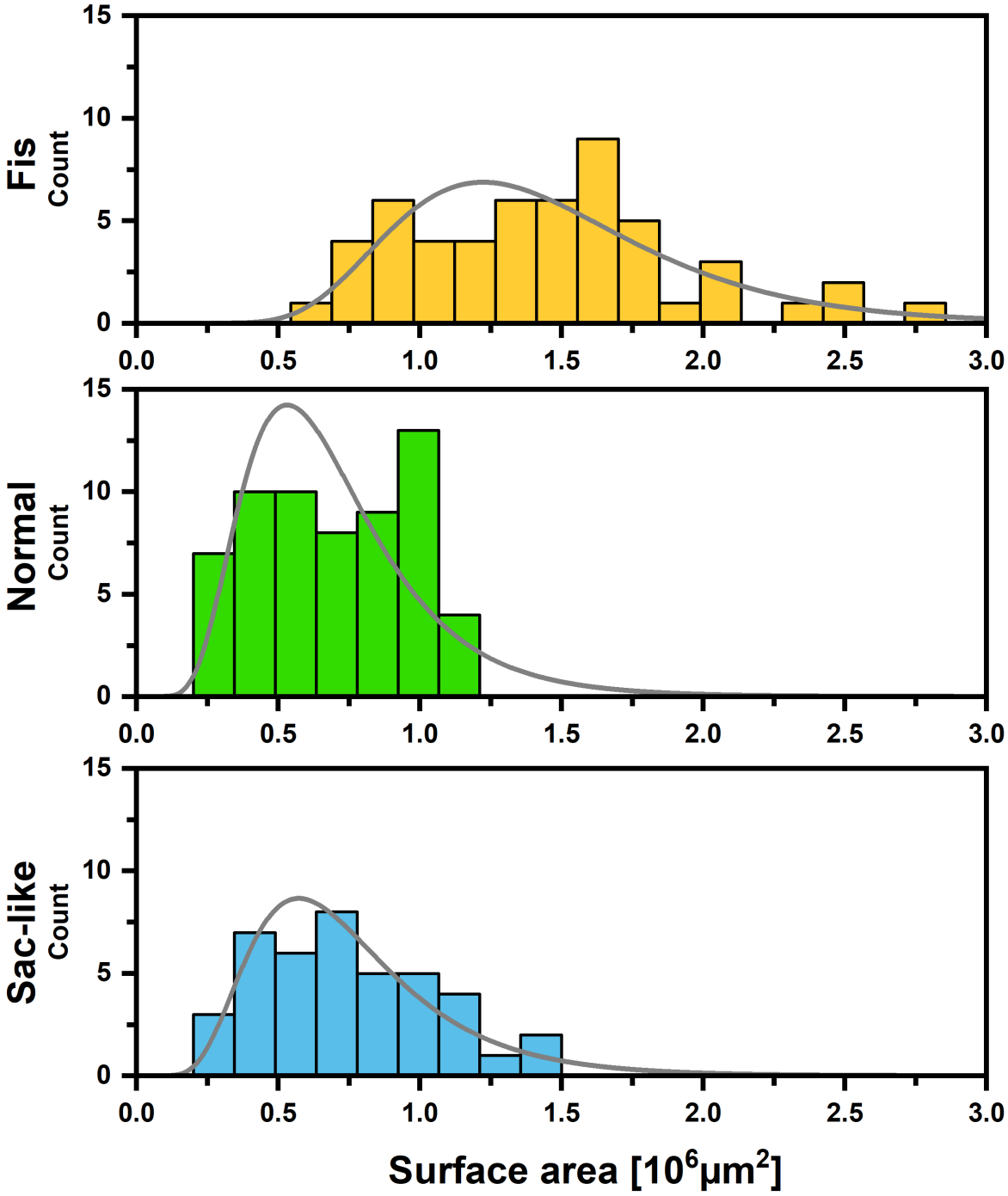

doi:10.6342/NTU202404142

Figure 3.4 Histogram and line graph for the surface area distribution of Fis (the orange histogram in the top), Normal (the green histogram in the middle) and Sac-like (the blue histogram in the bottom) forms. It shows the variation of sample distribution across Fis, Normal and Sac-like forms.

3.3 Surface-total volume (S-V) ratio

3.3.1 Distribution of *G. fistulosa* (Fis form)

Totally 53 *G. fistulosa* (Fis form**)** specimens are included. The data are plotted in the boxplot (Figure 3.5) and the histogram (Figure 3.6) to show the S-V ratio distribution, with the partial descriptive statistics summarized in table 3.3. The value of data is ranging from $1.2x10^{-2}$ $\mu m^{(-1)}$ to $2.10x10^{-2}$ $\mu m^{(-1)}$, with mean at $1.53x10^{-2}$ $\mu m^{(-1)}$ and standard deviation at $2.29x10^{-3}$ μm^{-1}.

3.3.2 Distribution of *T. sacculifer* (Normal form)

Totally 61 *T. sacculifer* **(**Normal form**)** specimens are included. The data are plotted in the boxplot (Figure 3.5) and the histogram (Figure 3.6) to show the S-V ratio distribution, with the descriptive statistics summarized in Table 3.3. The value of data is ranging from $1.32x10^{-2}$ $\mu m^{(-1)}$ to $2.44x10^{-2}$ $\mu m^{(-1)}$, with mean at $1.77x10^{-2}$ μm^{-1} and standard deviation at $3.27x10^{-3}$ $\mu m^{(-1)}$.

3.3.3 Distribution of *T. sacculifer* (Sac-like form)

Totally 41 *T. sacculifer* **(**Sac-like form**)** specimens are included. The data are plotted in the boxplot (Figure 3.5) and the histogram (Figure 3.6) to show the S-V ratio distribution,

doi:10.6342/NTU202404142

with the descriptive statistics summarized in table 3.3. The value of data is ranging from $1.30x10^{-2}$ $\mu m^{(-1)}$ to $2.35x10^{-2}$ $\mu m^{(-1)}$, with mean at $1.76x10^{-2}$ $\mu m^{(-1)}$ and standard deviation at $3.25x10^{-3}$ $\mu m^{(-1)}$.

3.3.4 Comparison between *G. fistulosa* and *T. sacculifer* (Fis, Normal and Sac-like forms)

The S-V ratio comparison in between Fis vs. Normal, Fis vs. Sac-like and Normal vs. Sac-like forms are made with mean value and Two-sample student t-test. By comparing the mean value, in Fis vs. Normal group, the mean value in Fis is about 87 % as large as Normal, In Fis vs. Sac-like group, the mean value in Fis is about 87.5 % as larger as Sac-like. In Normal vs. Sac-like group, Sac-like form is 99.4% as big as Normal form. As for the result of the Two-sample student t-test, Fis form shows significant difference to both Normal and Sac-like forms. As for the comparison of Normal vs. Sac-like forms, the result shows no significant difference in between the two. The detailed result of the t-test is attached in Appendix 1.7-1.9 and the complete descriptive statistics is attached in Appendix 2.3.

doi:10.6342/NTU202404142

Table 3.3 Descriptive statistical comparison of the S-V ratio of Fis, Normal and Sac-like forms.

	G. fistulosa **(Fis form)**	***T. sacculifer*** **(Normal form)**	***T. sacculifer*** **(Sac-like form)**
Mean	1.53×10^{-2} μm^{-1}	1.77×10^{-2} μm^{-1}	1.76×10^{-2} μm^{-1}
Standard deviation	2.29×10^{-3} μm^{-1}	3.27×10^{-3} μm^{-1}	3.25×10^{-3} μm^{-1}
Minimum	1.2×10^{-2} μm^{-1}	1.32×10^{-2} μm^{-1}	1.30×10^{-2} μm^{-1}
Maximum	2.10×10^{-2} μm^{-1}	2.44×10^{-2} μm^{-1}	2.35×10^{-2} μm^{-1}
Sample numbers	53	61	41

doi:10.6342/NTU202404142

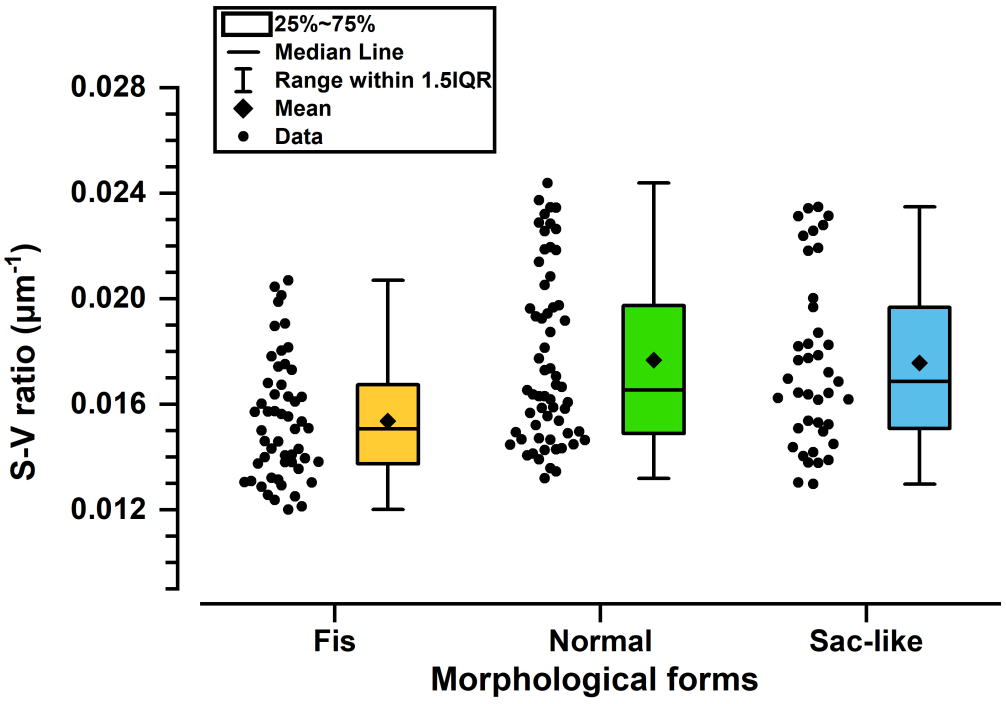

Figure 3.5 Boxplot for the surface area to total volume (S-V) ratio distribution of Fis (the orange box in the left), Normal (the green box in the middle) and Sac-like (the blue box in the right) forms. Each form is presents with the box of 25^{th}-75^{th} percentile, median line, range within 1.5IQR (range in between maximum and minimum values), mean point (filled diamond) and data point (filled circle). Based on the result of student t-test, Fis form is showing predominantly different distribution compare to the others, while Normal and Sac-like forms are showing no significant difference from each other.

doi:10.6342/NTU202404142

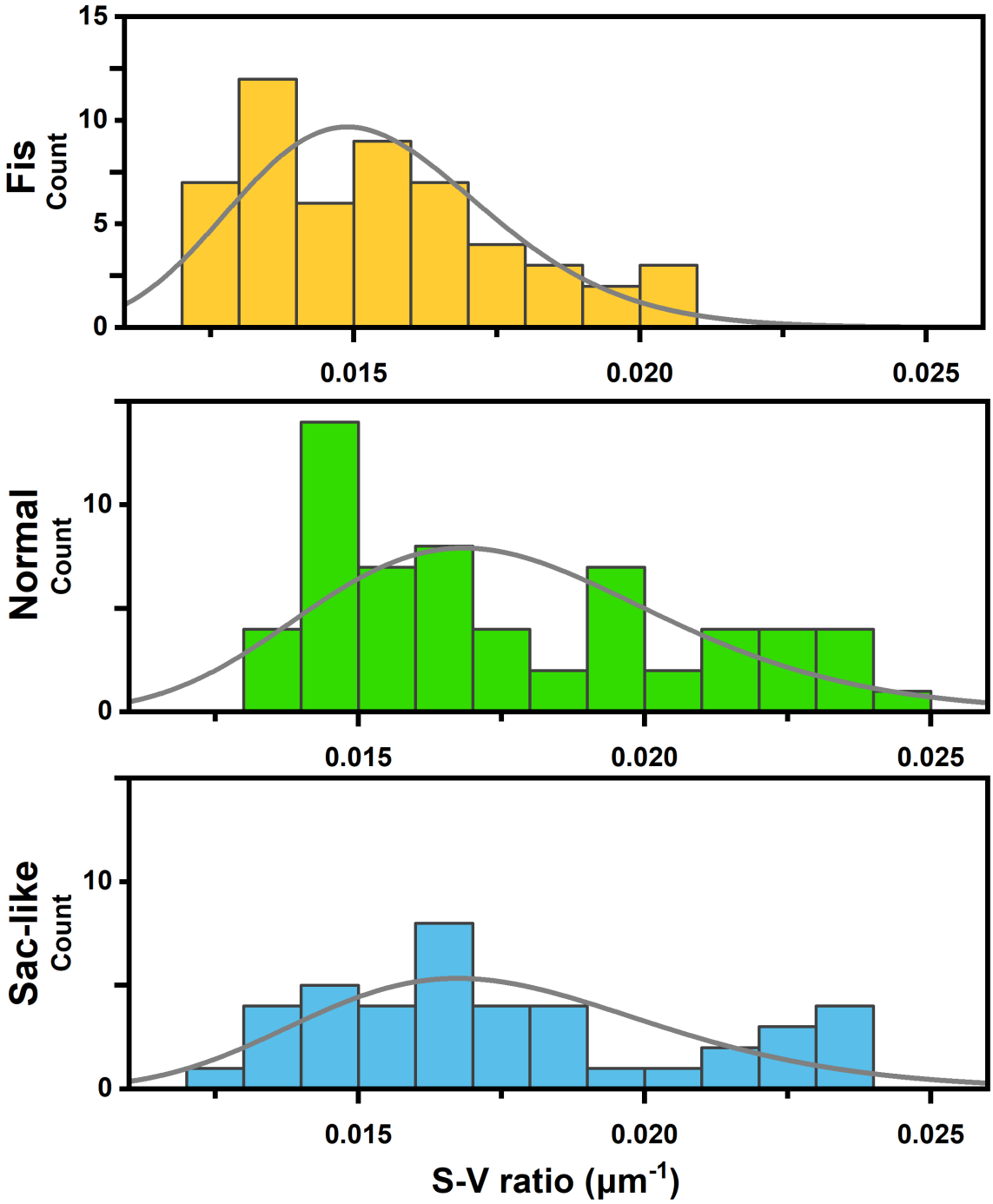

doi:10.6342/NTU202404142

Figure 3.6 Histogram and line graph for the Surface area to total volume (S-V) ratio distribution of Fis (the orange histogram in the top), Normal (the green histogram in the middle) and Sac-like (the blue histogram in the bottom) forms. It shows the variation of sample distribution across Fis, Normal and Sac-like forms.

3.4 Total volume-surface area relationship

By comparing the total volume with surface area, linear relationships are found on the three forms as shown in figures 3.7 and 3.8. Despite using exponential ExpDec3 model provided in the software *origin* for creating regression fits, the results). Highly similar regression patterns are found on Normal and Sac-like forms, as they are nearly perfectly overlapped on the data distribution and the regression fits. For Fis form, higher variation is found on surface area as the total volume increases. The equation formula of the regression fits for Fis, Normal and Sac-like forms are shown respectively in Figure 3.8 with the R-square values at 0.9340, 0.9900 and 0.9900. To be noted, Fis form registers larger variation in in test area as maximum test size increases. compared to the other forms, as the data distribution is loosely clustered.

To provide validity for the data, a dataset of planktonic foraminifera species *O. universa* from four size fractions is provided in Figure 3.9. Since the gross morphology of the last chamber of the species highly resembles sphere. The distribution of *O. universa* across size fractions approaches the exponential S-V ratio/total volume relationship of sphere as surface area/total volume=3/(radius of the last chamber). It should be pointed out that the

doi:10.6342/NTU202404142

distribution is not strictly follows sphere, as the gross morphology is slightly flatted as ellipsoid.

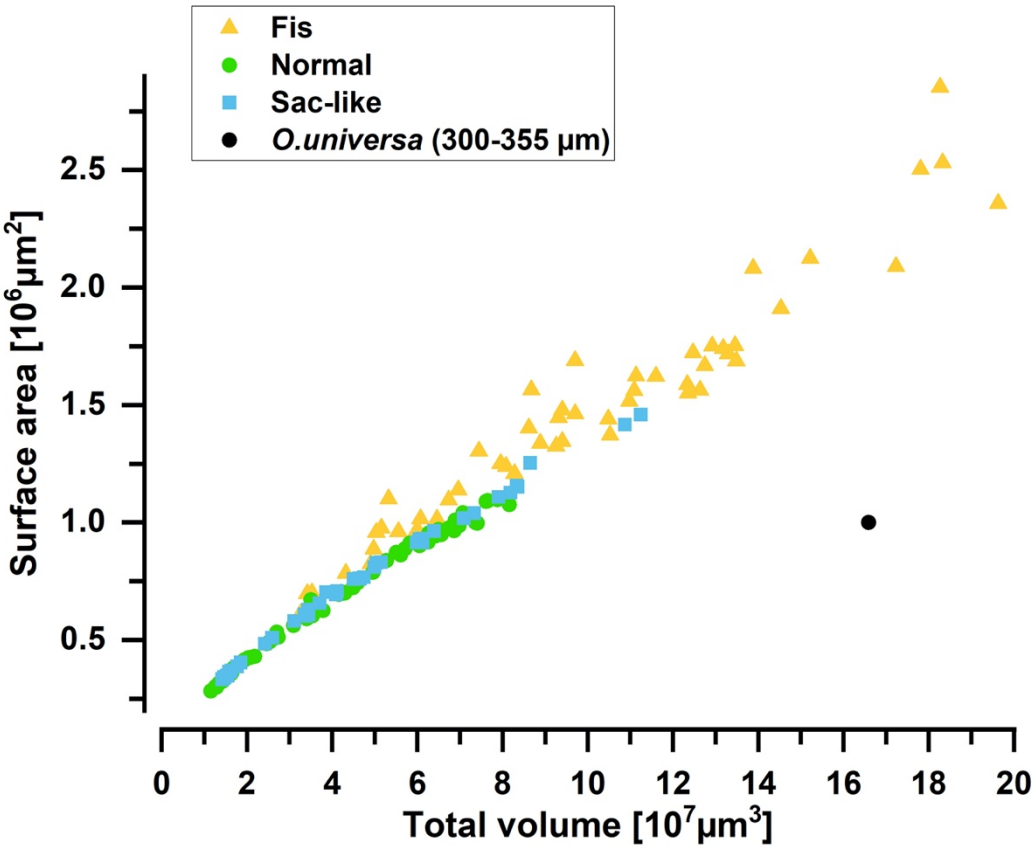

Figure 3.7 Scatterplot for the total volume-surface area distribution of Fis (the orange spots), Normal (the green spots) and Sac-like (the blue spots) forms. High consistency is found between Normal and Sac-like forms upon their distribution. For Fis form, it roughly follows a similar trend, albeit with significantly higher variation on surface area as the total volume increases.

doi:10.6342/NTU202404142

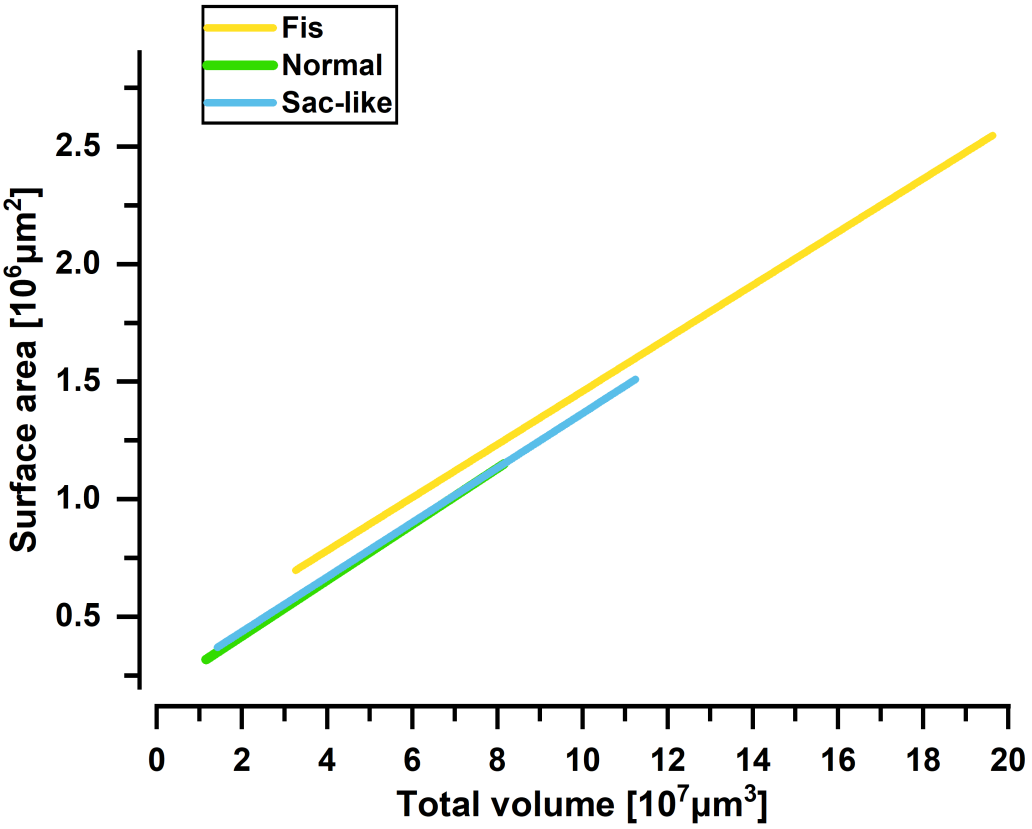

Figure 3.8 Linear regression fits for the total volume-surface area distribution of Fis (the orange line), Normal (the green line) and Sac-like forms (the blue line). High R-square values and similar increase rate for surface area as the total volume increases are found on all of the forms. To be noted, Fis form registers larger surface area compared to the others.

doi:10.6342/NTU202404142

Table 3.4 Equations of the regression fits of Fis, Normal and Sac-like forms for the total volume-surface area distribution.

Form	Fis	Normal	Sac-like
Equation	y = a + b*x	y = a + b*x	y = a + b*x
a	0.32981 ± 0.04474	0.18084 ± 0.00748	0.20543 ± 0.00876
b	0.11292 ± 0.00415	0.11893 ± 0.00168	0.116 ± 0.00162
R-square	0.9340	0.9990	0.990

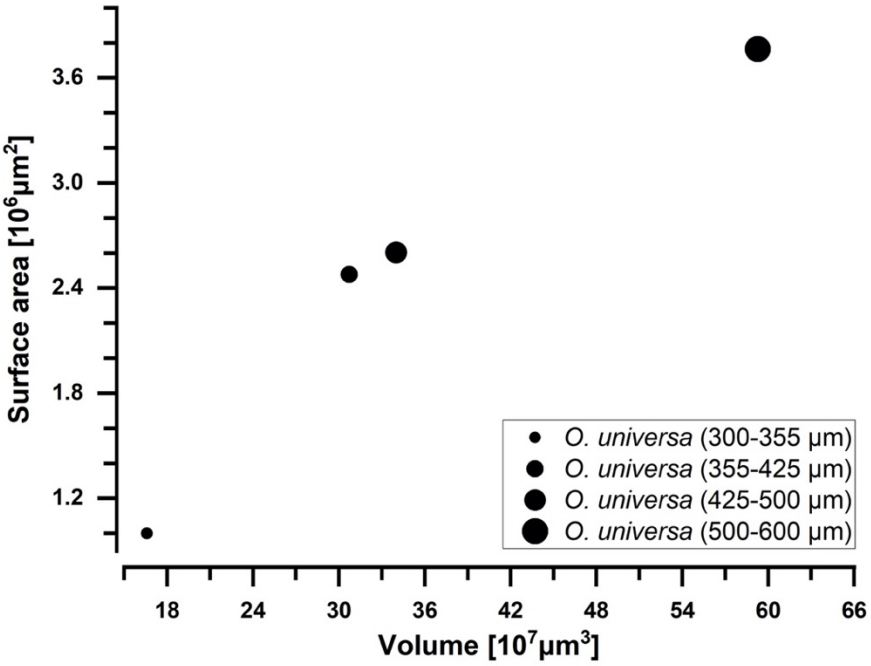

Figure 3.9 Scatterplot for the total volume-surface area distribution of *O. universa* from different size fractions (300-355, 355-425, 425-500 and 500-600 μm).

doi:10.6342/NTU202404142

3.5 Total volume-SV ratio relationship

With the comparison between volume and S-V ratio, strong decay exponential relationships are shown for the three forms in figure 3.10 and 3.11. Highly similar regression patterns are found on Normal and Sac-like forms, as they are nearly perfectly overlapped on the data distribution and the regression fits. For Fis form, a more right-shifted exponential relationship is shown compared to the other two. The equation formula of the regression fits for Fis, Normal and Sac-like forms are shown respectively in figure 3.11 with the R-square values at 0.7687, 0.9860 and 0.9943. To be noted, Fis form registers larger variation compared to the other forms, as the data distribution is loosely clustered in lower R-value of the regression fit.

To provide validity for the data, a dataset of *O. universa* from four size fractions is provided in figure 3.12.

doi:10.6342/NTU202404142

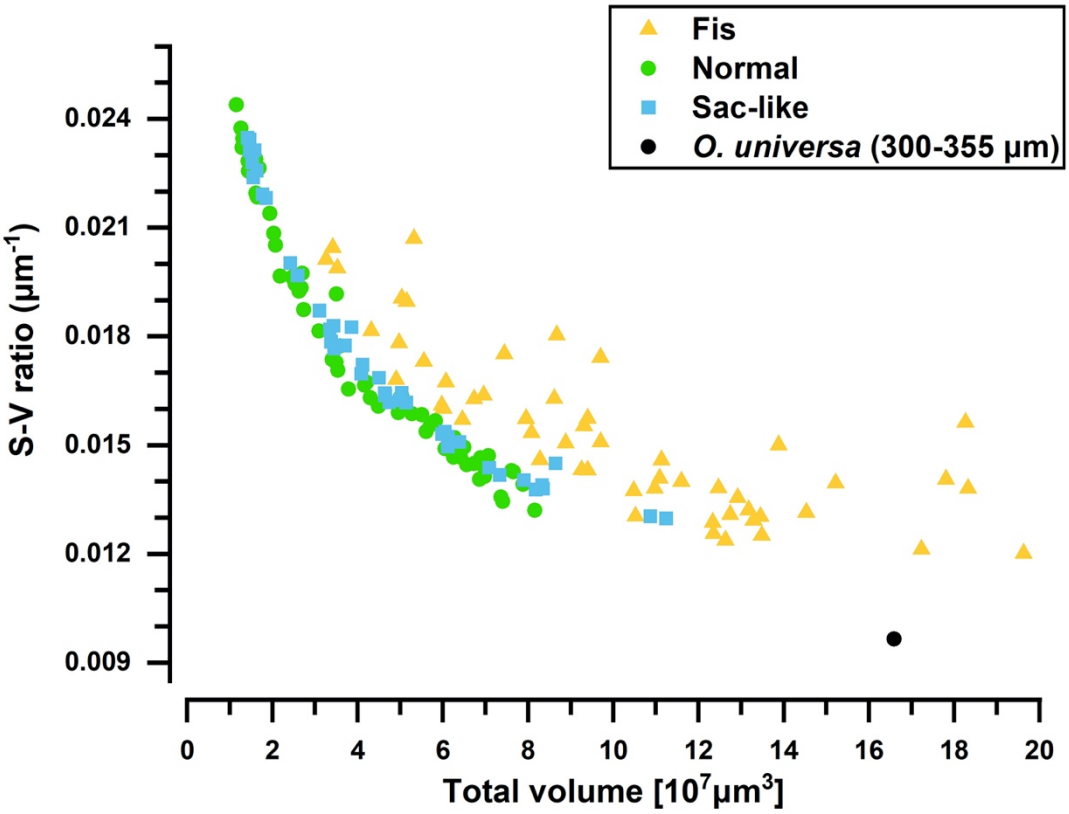

Figure 3.10 Scatterplot for the total volume-s-v ratio distribution of Fis (the orange spots), Normal (the green spots) and Sac-like (the blue spots) forms. High consistency is found between the Normal and Sac-like forms upon their distribution. For Fis form, it roughly follows a similar trend, albeit with significantly higher variation on surface area as the total volume increases.

doi:10.6342/NTU202404142

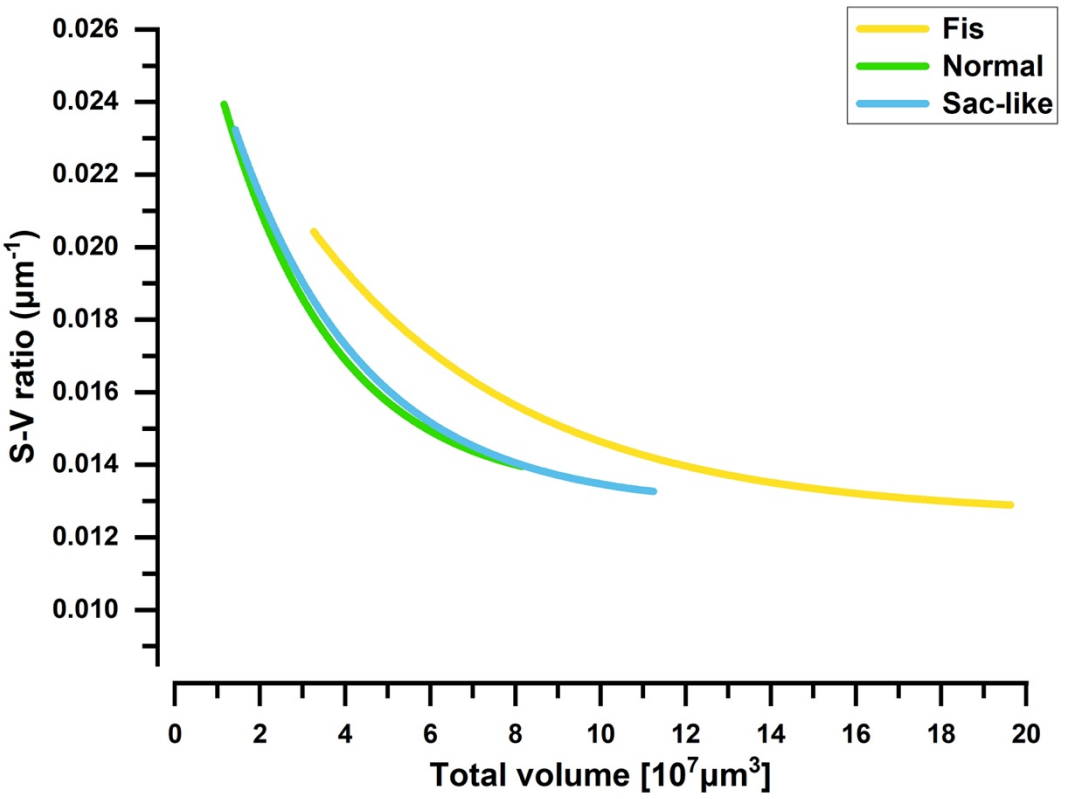

Figure 3.11 Exponential decay regression fits for the total volume-s-v ratio distribution of Fis (the orange line), Normal (the green line) and Sac-like forms (the blue line). High R-square values, consistency and similar decrease rate for S-V ratio as the total volume increases are found on the Normal and Sac-like forms. For Fis form, it roughly follows the trend with much higher variation on the S-V ratio as the total volume increases. the R-square value of Fis form is much lower than the other two forms. To be noted, Fis form registers larger S-V ratio compared to the others under the same total volume.

doi:10.6342/NTU202404142

Table 3.5 Equations of the regression fits of Fis, Normal and Sac-like forms for total volume-S-V ratio relationship.

Form	Fis	Normal	Sac-like
Equation	y = y0 + A1*exp(-x-x0/t1)	y = y0 + A1*exp(-x-x0/t1)	y = y0 + A1*exp(-x-x0/t1)
y0	0.01259 ± 6.23364E-4	0.01315 ⩽ 2.58877E-4	0.01284 z 1.91094E-4
x0	3.39216	0.90772	1.35406
A1	0.00763	0.01183	0.0106
t1	5.02789	2.68647	3.05965
R-square	0.76295	0.9829	0.99211

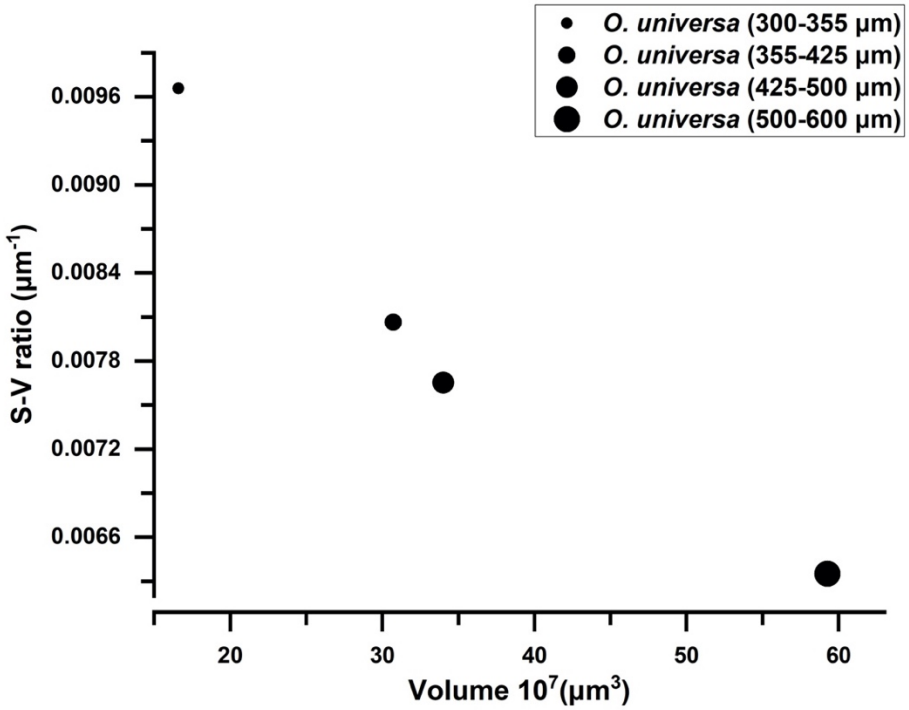

Figure 3.12 Scatterplot for the total volume-s-v ratio distribution of *O. universa* from different size fractions (300-355, 355-425, 425-500 and 500-600 μm). The distribution of *O.*

doi:10.6342/NTU202404142

universa across size fractions approaches the surface area/total volume relationship of sphere (assuming *O. universa* is always perfectly resembles sphere) as surface area/total volume=3/radius of the last chamber. This provides the validity of the data in this study.

3.6 Total volume distribution across different size fractions for the three forms

Based on the data presented in figures 3.13, 3.14 and 3.15, the volume distribution of Fis, Normal and Sac-like forms are described as followed. The range of every size fraction tend to increases as the size fraction increases. All of the smallest size fraction of every form has very small volume range, especially Fis form. The smallest size fractions ranging from $3.72x10^6$ (μm^3) to $2.23x10^7$ (μm^3). The range of total volume in nearly all of the size fractions of the three forms are partially overlapped, especially in the size fractions larger than the second smallest size fraction. Considering the value of median as the representative parameter, the volume growth rate in between every two consecutive size fractions varies. Some outliers are found for Normal and Sac-like forms, which may be attributed to incompleteness of the data across all size fractions available.

doi:10.6342/NTU202404142

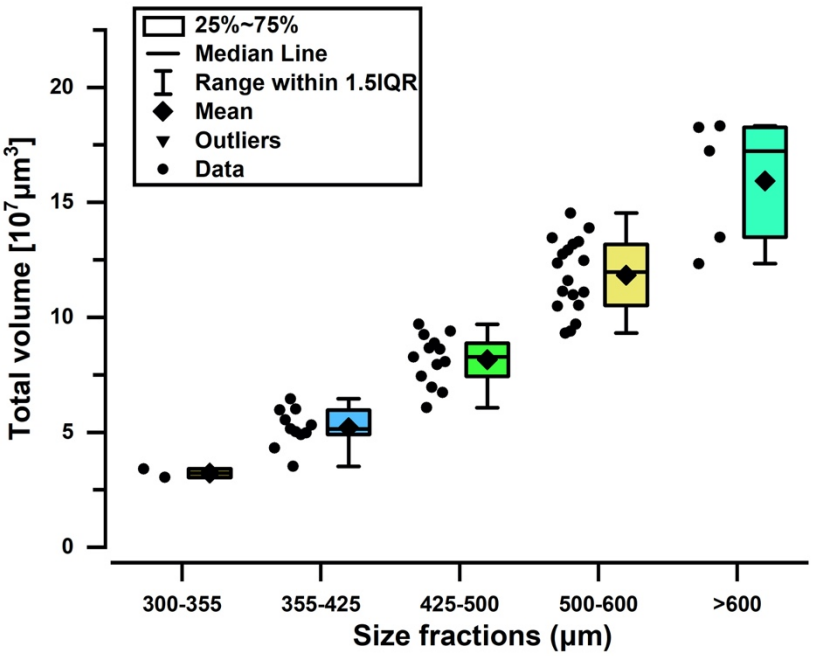

Figure 3.13 Boxplot for the volume distribution of *G. fistulosa* (Fis form) across size fractions. Five size fractions are included in the figure: 300-355 µm (the brown box), 355-425 µm (the blue box), 425-500 µm (the dark green box), 500-600 µm (the orange box) and >600 µm (the light green box). The range of size fraction increases as the size fraction becomes larger.

doi:10.6342/NTU202404142

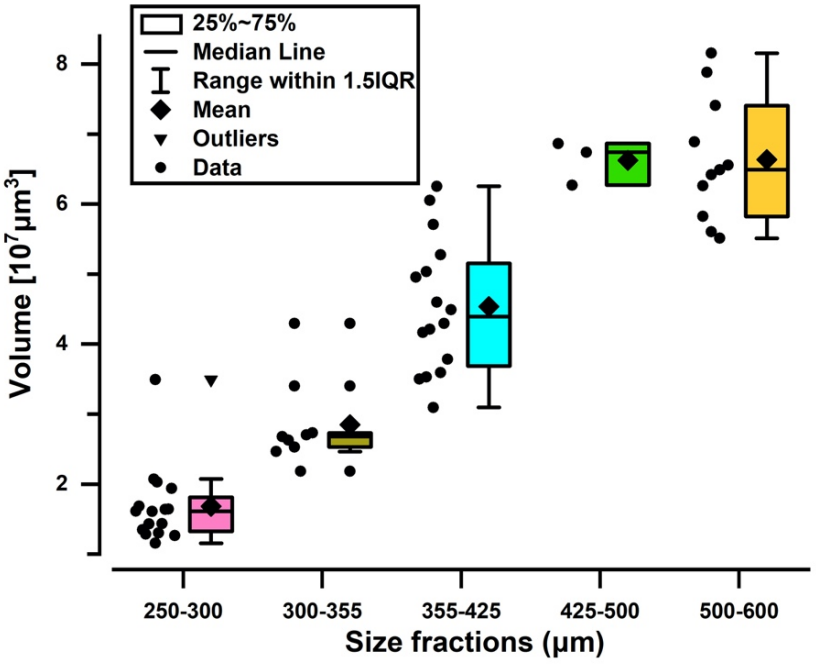

Figure 3.14 Boxplot for the volume distribution of *T. sacculifer* (Normal form) across different size fractions. Five size fractions are included in the figure: 250-300 μm (the pink box), 300-355 μm (the brown box), 355-425 μm (the blue box), 425-500 μm (the green box) and 500-600 μm (the orange box). The range of every size fraction seems maintain constant in between 2-2.5 (10^7 μm³) except the fraction of 425-500 μm.

doi:10.6342/NTU202404142

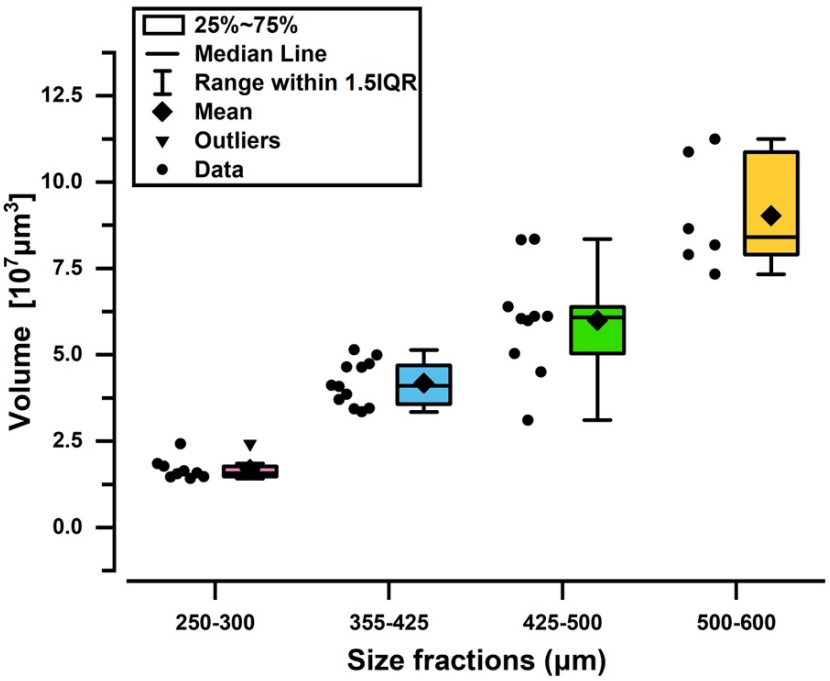

Figure 3.15 Boxplot for the volume distribution of *T. sacculifer* (Sac-like form) across different size fractions. Four size fractions are included in the figure: 250-300 μm (the pink box), 355-425 μm (the blue box), 425-500 μm (the green box) and 500-600 μm (the orange box). The range of size fraction increases as the size fraction becomes larger.

doi:10.6342/NTU202404142

3.7 Surface area distribution across different size fractions for the three forms

Based on the data presented in figures 3.16, 3.17 and 3.18, the surface area distribution of Fis, Normal and Sac-like forms are described as followed. The range of the size fraction of Fis form tends to increases as the size fraction increases. For Normal and Sac-like forms, no significant surface area-size relationships are observed. All of the smallest size fraction of every form tends to have smaller surface area range compared to the size fraction with highest range, especially Fis form. The range of surface area in nearly all of the size fractions of the three forms are partially overlapped. Considering the value of median as the representative parameter, the surface area growth rate in between every two consecutive size fractions varies. Some outliers are found for all of the three forms, which may be attributed to incompleteness of the data across all size fractions available.

doi:10.6342/NTU202404142

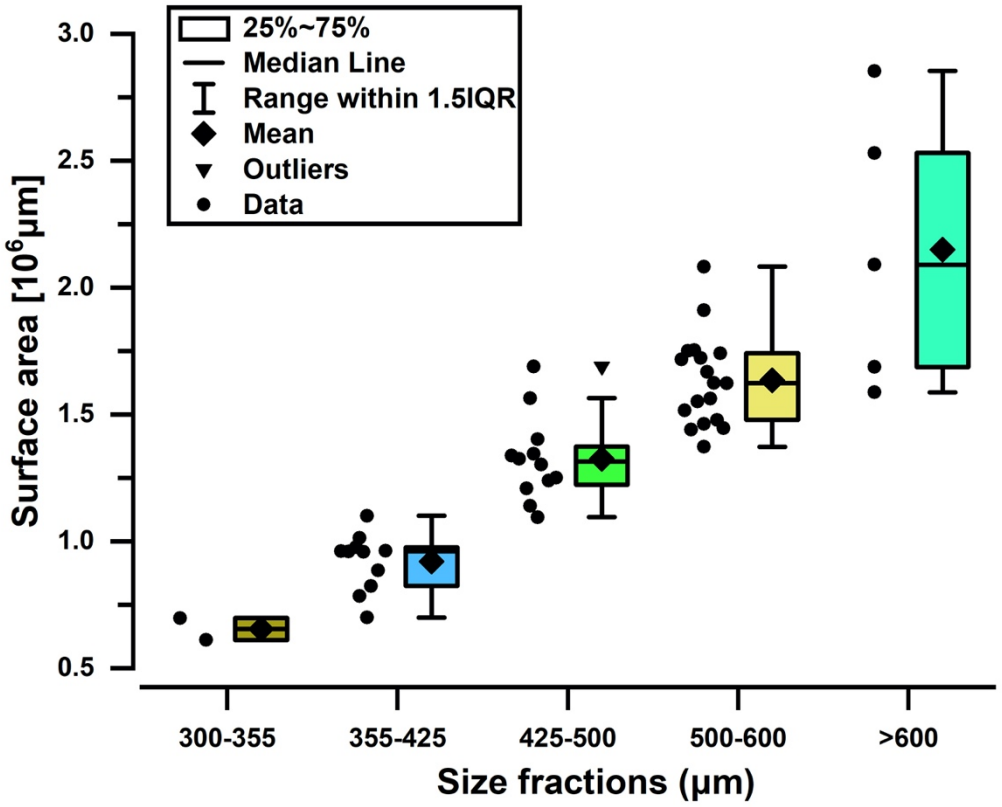

Figure 3.16 Boxplot for the surface area distribution of *G. fistulosa* (Fis form) across size fractions. Five size fractions are included in the figure: 300-355 µm (the brown box), 355-425 µm (the blue box), 425-500 µm (the dark green box), 500-600 µm (the orange box) and > 600 µm (the light green box). The range of size fraction increases as the size fraction becomes larger.

doi:10.6342/NTU202404142

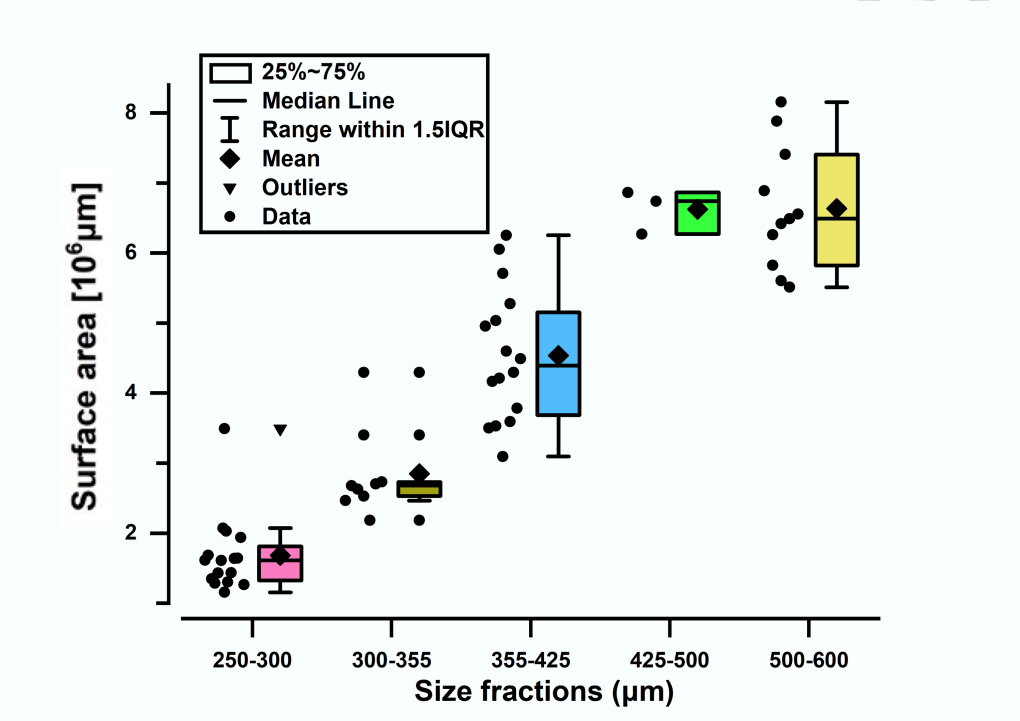

Figure 3.17 Boxplot for the surface area distribution of *T. sacculifer* (Normal form) across different size fractions. Five size fractions are included in the figure: 250-300 μm (the pink box), 300-355 μm (the brown box), 355-425 μm (the blue box), 425-500 μm (the green box) and 500-600 μm (the orange box). No significant trend found for the size fraction increases as the size fraction becomes larger.

doi:10.6342/NTU202404142

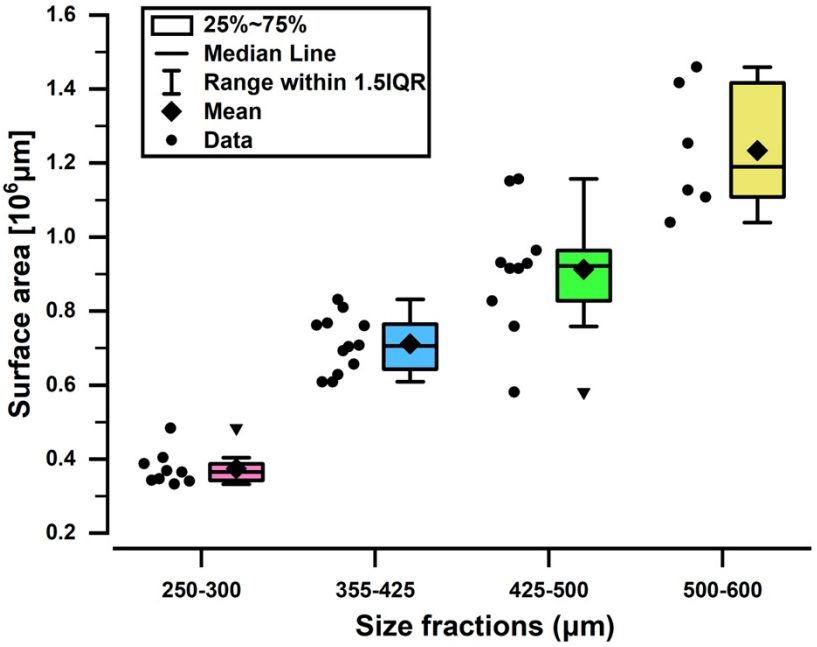

Figure 3.18 Boxplot for the surface area distribution of *T. sacculifer* (Sac-like form) across different size fractions. Four size fractions are included in the figure: 250-300 μm (the pink box), 355-425 μm (the blue box), 425-500 μm (the green box) and 500-600 μm (the orange box). The range of size fraction seems increases as the size fraction becomes larger.

doi:10.6342/NTU202404142

3.8 Surface-total volume (S-V) ratio distribution across different size fractions for the three forms

Based on the data presented in figures 3.19, 3.20 and 3.21, the surface-total volume (S-V) ratio distribution of Fis, Normal and Sac-like forms are described as followed. For all the three forms, no significant surface area-size relationships are observed. All of the smallest size fraction of every form tends to have smaller volume range compared to the size fraction with highest range, especially Fis form. The range of total volume in nearly all of the size fractions of the three forms are partially overlapped. Some outliers are found for the Normal and Sac-like forms, which may be attributed to incompleteness of the data across all size fractions available.

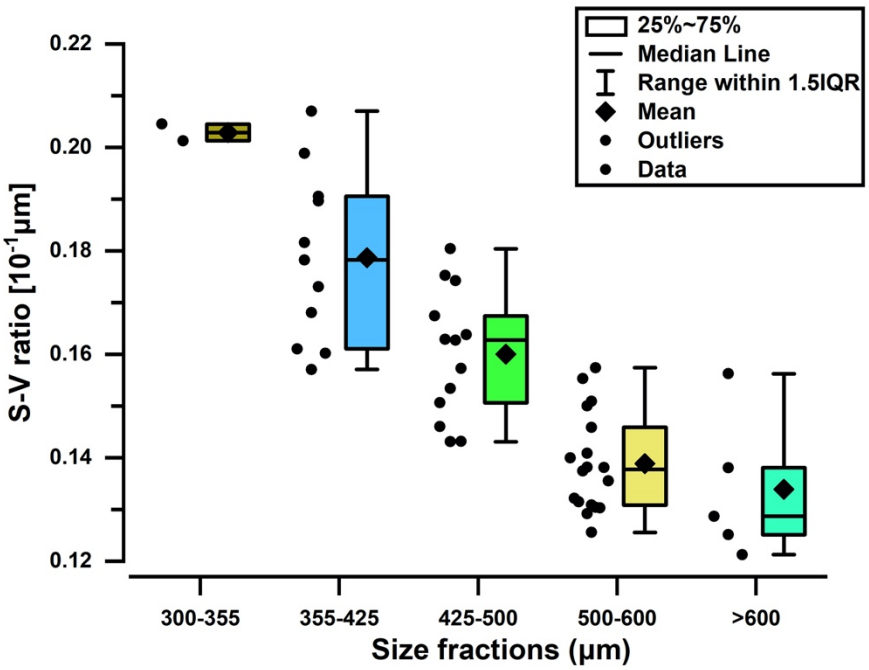

doi:10.6342/NTU202404142

Figure 3.19 Boxplot for the S-V ratio distribution of T. sacculifer (Sac-like form) across different size fractions. Five size fractions are included in the figure: 250-300 μm (the pink box), 355-425 μm (the blue box), 425-500 μm (the green box) and 500-600 μm (the orange box). No significant trend found for the size fraction increases as the size fraction becomes larger.

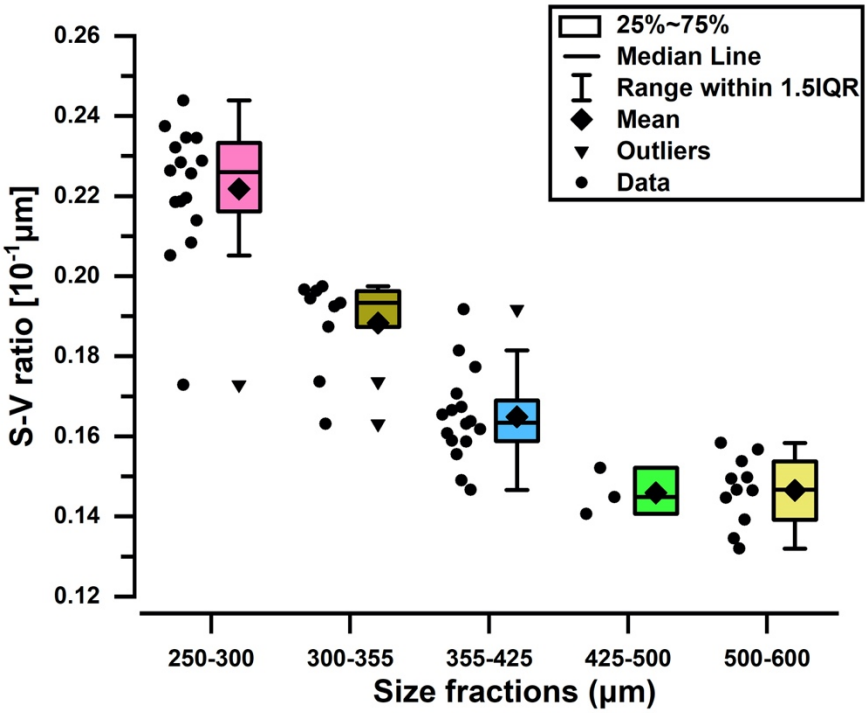

Figure 3.20 Boxplot for the S-V ratio distribution of *T. sacculifer* (Normal form) across different size fractions. Five size fractions are included in the figure: 250-300 μm (the pink box), 300-355 μm (the brown box), 355-425 μm (the blue box), 425-500 μm (the green box) and 500-600 μm (the orange box). No significant trend found for the size fraction increases as the size fraction becomes larger.

doi:10.6342/NTU202404142

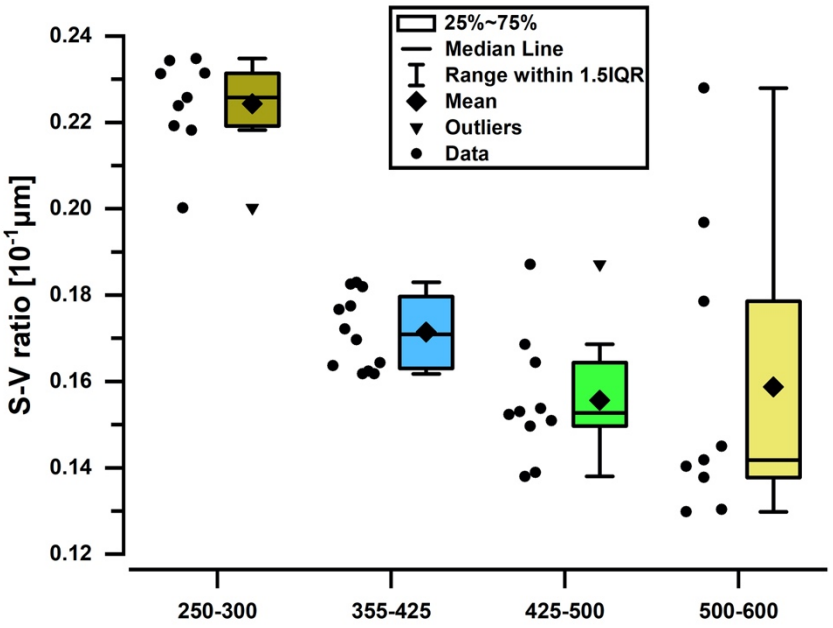

Figure 3.21 Boxplot for the S-V ratio distribution of *T. sacculifer* (Sac-like form) across different size fractions. Four size fractions are included in the figure: 250-300 μm (the pink box), 355-425 μm (the blue box), 425-500 μm (the green box) and 500-600 μm (the orange box). No significant trend found for the size fraction increases as the size fraction becomes larger.

doi:10.6342/NTU202404142

Chapter 4: Discussion

4.1 Data variation

4.1.1 Total volume

G. fistulosa (Fis form) is showing overwhelmingly larger volume compared to the other two forms, as the largest individual of the *G. fistulosa* (Fis form) is around two times larger than both of Normal and Sac-like forms. The result could be attributed to the increased number of chambers, the presence of digitate protuberance (s), and the larger chamber diameter of the last two to three chambers of *G. fistulosa* (Fis form). However, it should be pointed out that around half individuals of *G. fistulosa* (Fis form) overlapped with Normal and Sac-like forms in the interval in between around $3x10^7$-$8x10^7$ (μm^3).

The volume distributions of Normal and Sac-like forms are highly similar, only around five individuals of the Sac-like forms are larger than the interval of Normal form. As the rule to differentiate the two forms is the presence of the Sac-like last chamber, the volume variation of the Sac-like chamber may be the reason that caused the data variation. According to the current understanding to the modern *T. sacculifer*, the difference is caused by the Sac-like chamber growth right before the gametogenesis. Nevertheless, it is not an inevitable event happens before the gametogenesis.

4.1.2 Surface area

Likewise, *G. fistulosa* (Fis form) is showing overwhelmingly larger surface area compared to the other two forms, as the largest individual of Fis form is around or more than two times larger than both of Normal and Sac-like forms. In addition, only one-third of Fis

doi:10.6342/NTU202404142

form individuals are overlapped with Normal and Sac-like forms in the interval in between around $0.6x10^6$-$1.05x10^6$ (μm^2). The increased surface area of *G. fistulosa* (Fis form) could be attributed to its body size, especially the size of the last two chambers. A more flatted morphology compared to the other two forms could also be the possibility, as a more flatted shape can lead to the maximization of surface area over volume (Burke et al., 2020). An outlier is found at $3.07x10^5$ μm^2 for *G. fistulosa* (Fis form) in the boxplot. Interestingly, the total volume and the S-V ratio calculated based on this surface area and total volume value of the individual does not recognize as outliers. This implies the huge surface area variation presents on *G. fistulosa* (Fis form), as well as loss of fossil record that contains individuals with extreme values of surface area.

The surface area distributions of Normal and Sac-like forms are similar, while there are six individuals of the Sac-like forms are larger than the interval of Normal form. The slightly larger surface area of the Sac-like chamber on some individuals may be the reason that caused the data variation.

4.1.3 Surface-total volume (S-V) ratio

G. fistulosa (Fis form) is generally smaller than Normal and Sac-like forms on the surface-total volume ratio by comparing the value of mean and the maximum. The mean value of Fis form is around 86% of Normal and Sac-like forms. However, most of the individuals of Fis form are highly overlapped with Normal and Sac-like forms. Only less than five individuals are smaller than Normal form, and no individuals are smaller than the Sac-like form. The lower the S-V ratio is, more flatted the gross morphology is, as a more

doi:10.6342/NTU202404142

flatted shape can lead to the increase of surface area over volume (Burke et al., 2020). From the observation under microscope, the shape of the last chamber on Fis form tends to be flatted, which could alter the S-V ratio of the whole test. The protuberances appear on the chamber surface of the chamber could also be the reason by increasing surface area with little volume increased. However, it is probably not as influential as the chamber morphology.

The S-V ratio distributions of Normal and Sac-like forms are highly similar, while the Sac-like form is slightly smaller than Normal form by comparing the mean value. The flatted shell morphology of the Sac-like chamber on some relatively extreme individuals may be the reason that caused the data variation.

4.2 Data comparison and discussion with the previously reported data

4.2.1 Relative abundance data across different size fractions from Chen (2006)

Considering sieving size fractions (250-300, 300-355, 355-425, 425-500, 500-600 and larger than 600 μm) as a useful tool to estimate body size of planktonic foraminifera. Chen (2006) studied the body size distribution of *T. sacculifer* plexus (Normal, Kummer and Sac-like forms) and *G. fistulosa* (Fis form) using from a short time interval right before the LAD of *G. fistulosa*. By using samples from the same drilling site (ODP 1115B, the Solomon Sea) as this study, totally five horizons were covered from 1.757 Ma to 1.728 Ma. The result (Figure 4.1) shows *G. fistulosa* (Fis form) is only appears in the size fractions larger than 355 μm, the sample numbers tend to increase while size fraction is moving larger. Significantly, the it become dominant in the size fraction larger than 600 μm. However, Normal and Sac-like form of *T. sacculifer* are showing slightly different patterns with consistency to the

doi:10.6342/NTU202404142

modern *T. sacculifer*. The former tends to appears in the size fractions below 600 μm, with the sample numbers tend to decrease while size fraction is moving larger. The later appears in the size fractions below 600 μm, and the sample numbers tend to increase while size fraction is moving larger. Considering the observation, *G. fistulosa* is assumed to be part of the ontogenetic trajectory of *T. sacculifer*.

Chen's work provides critical clue to the morphospecific status of *G. fistulosa*. Nonetheless, the study directly assumes the interval of size fraction is representative to body size. While based on our measurement under 3D environment, the size fraction system is grouping samples with the short axis length of foraminifera test. For *G. fistulosa*, which generally larger than *T. sacculifer* on the long axis length, its body size could be underestimated under the size fraction system. Thus, the use of size fraction system may not be the best option to address the topic.

By comparing the total volume of Fis (*G. fistulosa*), Normal and Sac-like (*T. sacculifer*) forms in this study. Fis form tends to have larger total volume than Normal and Sac-like forms in the same size fraction by comparing the mean (figure 3.13-3.15). In addition, around half individuals of Fis form are larger than Normal and Sac-like (*T. sacculifer* plexus) forms on the total volume. The result supports and solidifies the possibility of *G. fistulosa* as the late ontogenetic stage (s) of *T. sacculifer*. Besides, environment-driven ecophenotypic variation could also be a possible assumption. The volume data also implies that, to access high fidelity for body size and biomass estimation, total volume or cumulative chamber volume would be better than size fraction.

doi:10.6342/NTU202404142

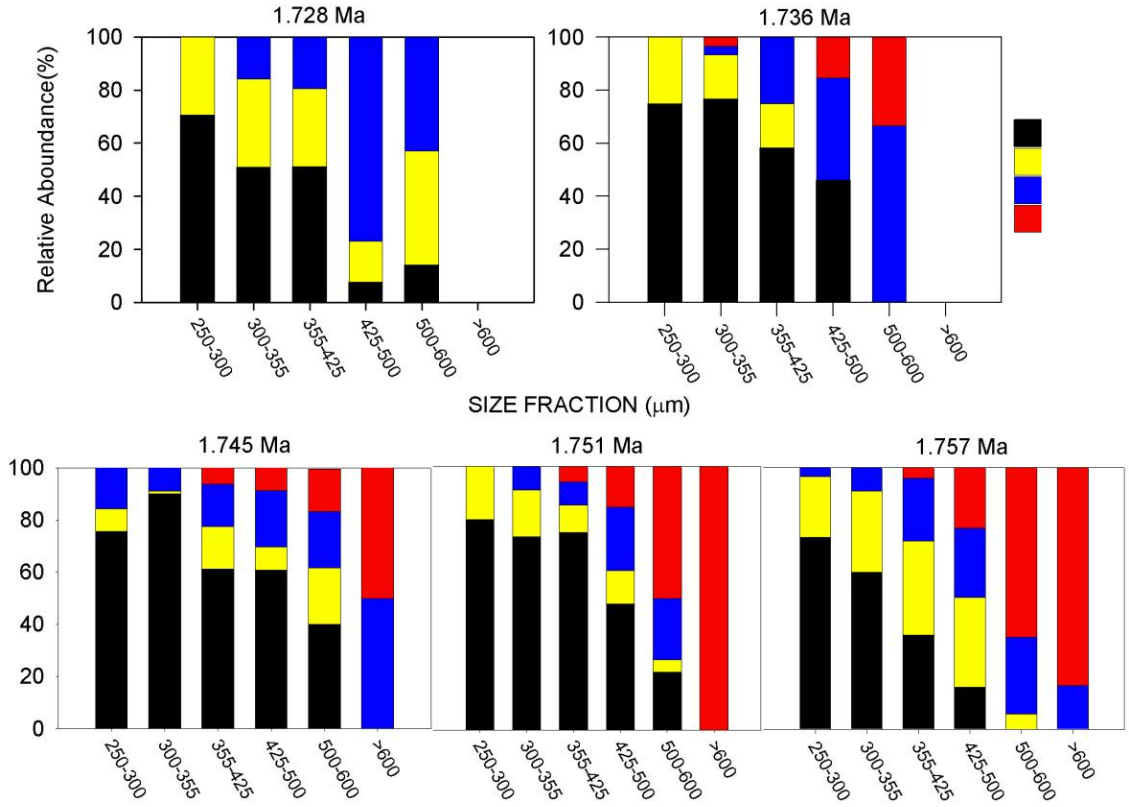

Figure 4.1 Relative abundance data across different size fractions of *T. sacculifer* plexus (Normal (black), Kummer (yellow) and Sac-like forms (blue)) and *G. fistulosa* (Fis form (red)). Figure revised from Chen (2006). *G. fistulosa* (Fis form) is only occurred in the size fraction larger than 355 μm, while *T. sacculifer* plexus is relatively smaller. The result implies the possibility of *G. fistulosa* (Fis form) as late ontogenetic stage (s) of *T. sacculifer* plexus. To be noted, the age model used in the study is different from the lately published integrated version (Chuang et al., 2018) and therefore further revision would be needed.

doi:10.6342/NTU202404142

4.2.2 Maximum test size-test surface area comparison from Poole and Wade (2019)

Poole and Wade (2019) summarized the systematics of *T. sacculifer* plexus (*T. trilobus*, *T. immaturus*, *T. quadrilobatus* and *T. sacculifer*) and *G. fistulosa*. Except the qualitative description for systematics, some quantitative data including maximum length of test and test surface area, were reported based on 2D photography. Exponential relationship was found on all of the morphospecies of the *T. sacculifer* plexus and *G. fistulosa* based on the comparison between maximum length of test and test surface area (Figure 4.2). For all of the morphospecies of the *T. sacculifer* plexus, the curves are with high R-square values (over 0.95). *G. fistulosa*, somehow, is characterized with a lower value (0.7863).

The strong exponential trend shown on the 2D data (Figure 4.2) is very different from the 3D data (Figures 3.7 and 3.8) reported in this study, and which could be attributed to the dimensional difference between the parameters used on the X and Y-axis, respectively. As test area has power of two compared to power of one on maximum length of test. The test area, without doubt, increases faster than maximum length of test. Apart from the exponential nature, the differences linked to the limitation of 2D photography is argued as bias here. Three exponential trends can be roughly recognized in different right-shifted extents: trend 1 for *T. trilobus* and *T. immaturus* (equal to Normal form) in the left, trend 2 for *T. quadrilobatus* and *T. sacculifer* (equal to Normal and Sac-like form) in the middle and trend 3 for *G. fistulosa* (equal to Fis form) in the right. For *T. trilobus* and *T. immaturus*, only three chambers can be observed under 2D perspective, and the two species are characterized with spherical last chamber. These characters result in smaller test surface area over maximum length of test. By contrast, *T. quadrilobatus* and *T. sacculifer* are characterized with four

doi:10.6342/NTU202404142

chambers observed under 2D perspective (*T. quadrilobatus*) and flat, sac-like last chamber (*T. sacculifer*). These characters result in relatively larger test surface area over maximum length of test, and lead to more right-shifted curves compared to the trend 1. For *G. fistulosa*, which's curve is observed to be more right-shifted. The presence of the protuberance could contribute a lot on its right-shift trend, as it brings about larger maximum test size over test surface area. In addition, *G. fistulosa* is observed to registers more variation in test surface area as maximum test size increases. This might be caused by the various chamber shape of *G. fistulosa*, which range from flat, sac-like, irregular shape to spherical and rounded shape. Such shape variation could be ignored as the measurement of test surface area is carried in 2D perspective. It seems that the extent of right-shift on these morphospecies is greatly depending on the geometry of chamber shape and chamber configuration of the morphospecies.

With additional information from Z-axis, the biases mentioned above can be corrected in the 3D data (Figure 3.7 and 3.8). Difference can hardly be found between Normal (*T. trilobus*, *T. immaturus* and *T. quadrilobatus*) and Sac-like (*T. sacculifer*) forms on the 3D data (Figure 3.7 and 3.8), as they are almost perfectly overlapped and clustered in high R-square values (over 0.95). Fis form (*G. fistulosa*), is found slightly depart from the other two forms, which could be attributed to more surface area variation as the total volume increases, and slightly higher surface area-total volume ratio. More variation is found on the surface area on Fis form as the total volume increases, as the characteristic is reflected on its lower R-square value (0.9381) compared to Normal and Sac-like forms. Nonetheless, it is not as

doi:10.6342/NTU202404142

much as the 2D data (R-square value=0.7863). As the result, two distinct trends are found respectively for Normal/Sac-like forms and Fis form.

4.2.3 Total volume-S-V ratio comparison

With the use of total volume as the body size indicator, we are able to discuss how the S-V ratio (surface-total volume ratio) changes through ontogeny for Fis, Normal and Sac-like forms (Figures 3.10 and 3.11). All of the three forms showing decreasing S-V ratio as the volume increases, which is consistent with the previously reported data (despite the parameter used in the previous study is cavity volume total volume; the parameter used for estimating body size is test length) (Caromel et al., 2016) (Figure 4.3). Two literally different trends are recognized: Densely distributed trend for Normal and Sac-like forms, and the scattered trend for Fis form. For Normal and Sac-like forms, they can hardly be differentiated as the two forms are similarly distributed and partially overlapped. Such result is quite understandable, as the two forms are currently considered to be the same biological species (*T. sacculifer*) (Bé, 1980). However, predominantly larger S-V ratio is found on Fis form compared to Normal and Sac-like forms under the same volume. Geometrically, the result might cause by the presence, shape and number of the digitate protuberance, as well as the general shape of the last chamber and the whole shell test. Further mathematic estimation would be needed to understand the contribution of every factor and what factors are relatively more influential.

Slight differences on the S-V ratio data reported in this study and the data in Caromel et al. (2016) are found on the materials of *T. sacculifer* plexus. For our data, the Sac-like (*T.*

doi:10.6342/NTU202404142

sacculifer) form is showing slightly larger surface area to total volume ratio than Normal form (*T. trilobus*, *T. immaturus*, *T. quadrilobatus*) under the same volume. While in Caromel et al. (2016), *T. trilobus* is slightly larger than *T. sacculifer* on the S-V ratio under the same test length (Figure 4.3). Since

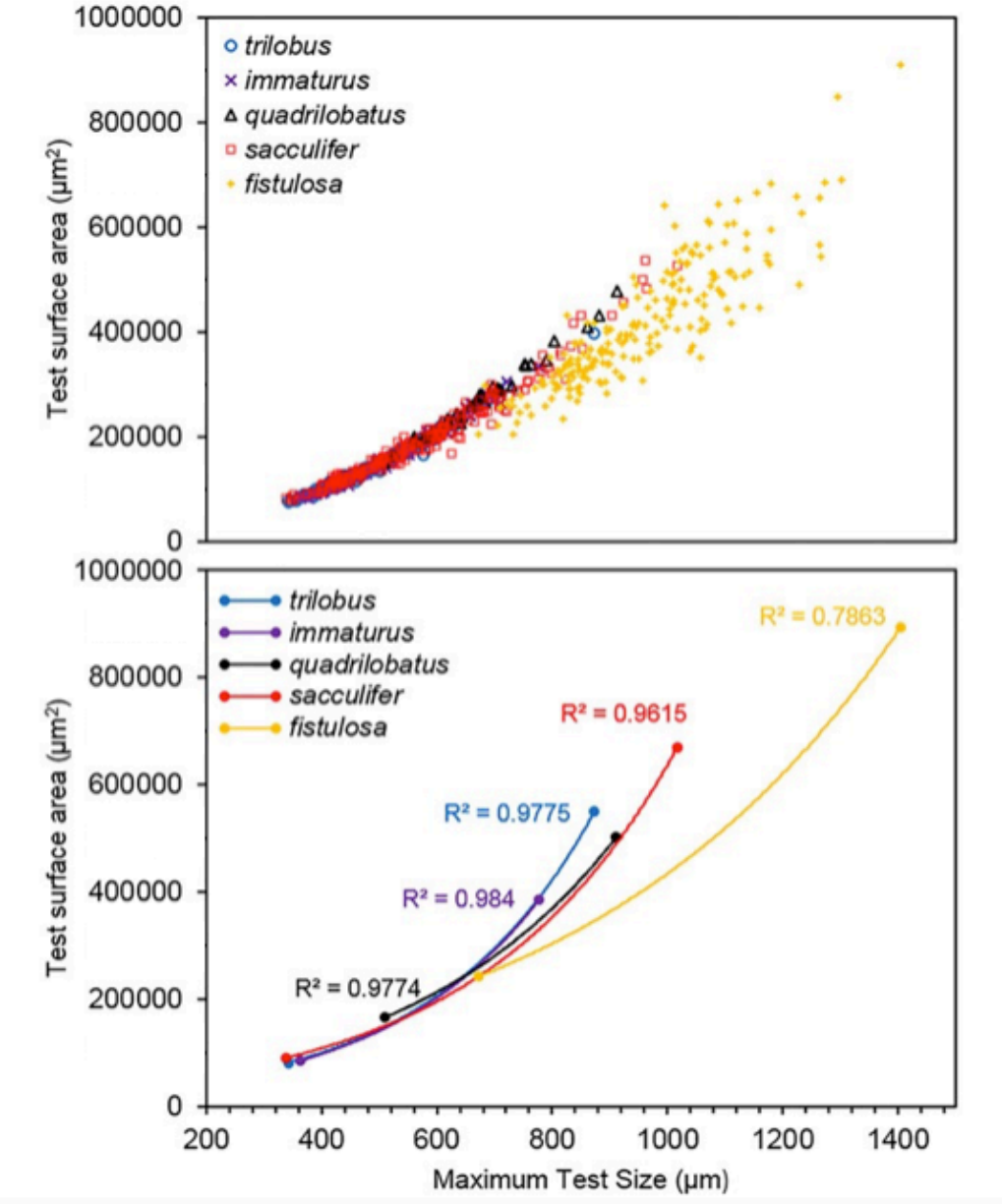

doi:10.6342/NTU202404142

Figure 4.2 Comparison of maximum test size and test surface area (raw data and regression lines) from Poole and Wade (2019) based on 2D data of *T. sacculifer* plexus (*T. trilobus*, *T. immaturus*, *T. quadrilobatus* and *T. sacculifer*) and *G. fistulosa*. The right-shifted trends are found on all the morphospecies of *T. sacculifer* plexus and *G. fistulosa*, which are considered biases of 2D photography.

Caromel et al. (2016) is using cavity volume to calculate its S-V ratio, slight interspecific variation occurs on test shell thickness could be the reason that cause the difference.

Unlike Normal and Sac-like forms, Fis form is showing larger S-V ratio variation by comparing individuals under the same volume. Such variation is also shown on the smaller R-square value (=0.7687). This might cause by the variation of chamber surface area, which is interpreted to be morphology-controlled. The gross morphology of Fis form ranging from sac-like, flat—which tends to increase surface area over volume—to rounded spherical shape—which tends to increase volume over surface area. Furthermore, the presence, number, length and thickness of protuberance could also play critical rule on increasing the surface area.

doi:10.6342/NTU202404142

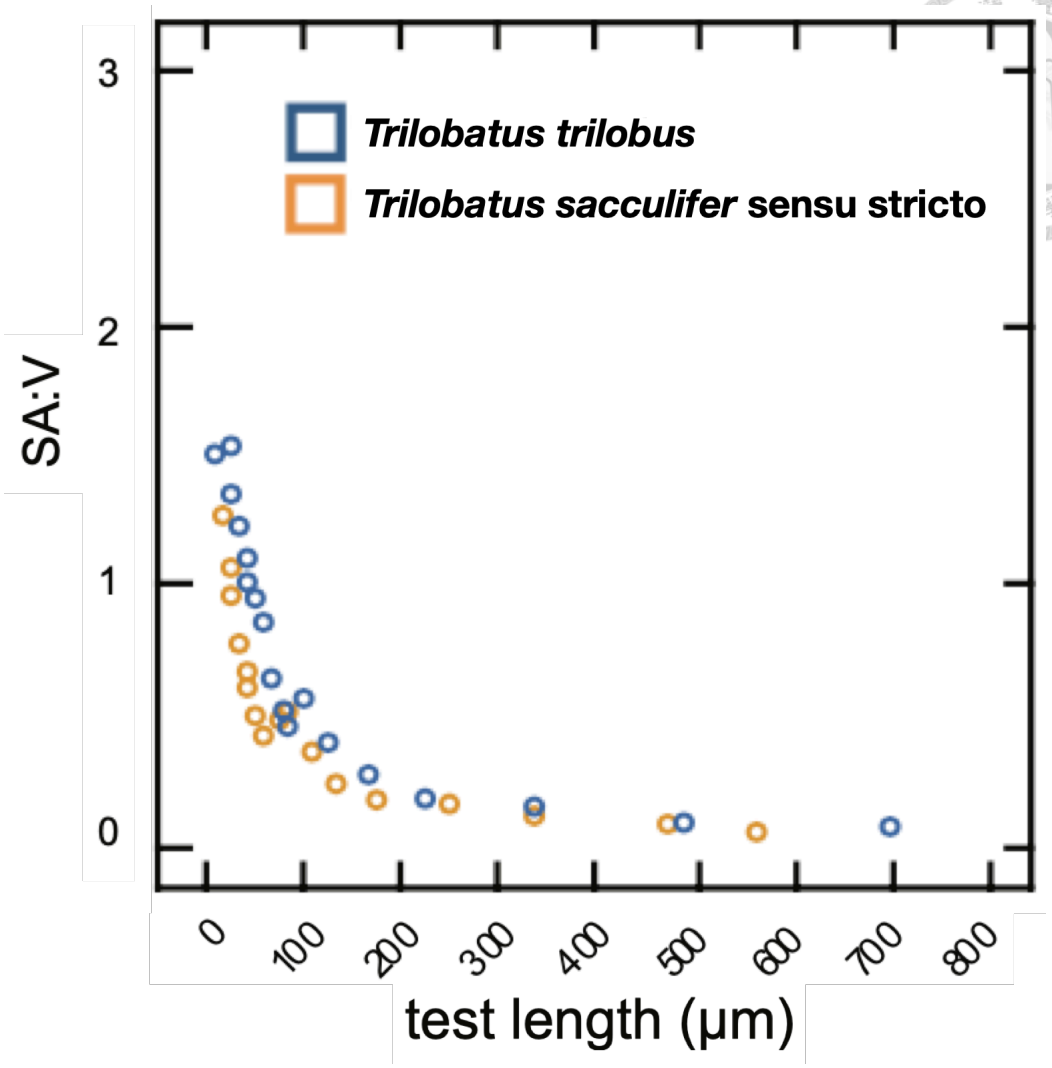

Figure 4.3 Comparison of surface area to test internal volume ratio and test length for *T. sacculifer* plexus. To be noted, the volume used in here is the test internal volume (the calcite test is not included in the calculation). Revised from Caromel et al.(2016).

doi:10.6342/NTU202404142

4.3 Adaptive functional morphology of *G. fistulosa* (Fis form)

As mentioned in section 4.2.2, two distinct total volume-surface growing trends are found through ontogeny: The highly consistent and densely distributed trend of Normal/Sac-like forms of *T. sacculifer* and sparsely scattered trend of Fis form (*G. fistulosa*). The three forms are sharing generally similar growth based on the regression analysis. Despite some individuals are following the growth pattern of *T. sacculifer*, most of Fis form (*G. fistulosa*) are register with strong variation on the surface area as total volume increases, which could be subjected to strong environmental control. Generally, larger S-V ratio is found on Fis form (*G. fistulosa*) compared to *T. sacculifer* under the same volume, which often refers to large surface area and more flatted gross morphology (Burke et al., 2020). Larger surface area is also found on many individuals with larger total volume, which exceeding the volume interval of *T. sacculifer.* Since surface area is critical to metabolism processes such as gas diffusion and respiration rate (Signes et al., 1993), the larger surface area of Fis form (*G. fistulosa*) compared to *T. sacculifer* and its strong variation could be related to the general oxygen deficiency of oxygen level at the lower part of the water column. The improved respiration rate by the larger surface area could improve the relatively low metabolic activity and higher its contribution to the positive $\delta^{13}C$-size relationship reported in Chen (2008). The larger S-V ratio on Fis form (*G. fistulosa*) could also be referred to enhanced symbiotic photosynthesis, as the surface area influences the abundance of symbionts on spinose planktonic foraminifers (Caromel et al., 2016).

The more flatted gross morphology is strongly linked to the larger surface area on Fis form (*G. fistulosa*). However, other than the gross morphology, the presence and number of

doi:10.6342/NTU202404142

the digitate protuberance could also be instrumental to provide additional surface area. In addition, spine holes have been reported on the protuberance of Fis form (*G. fistulosa*) (Poole and Wade, 2019), which strongly supports the presence of spine. As additional surface area and spines on the protuberance are found on Fis form (*G. fistulosa*), increased buoyancy and more space for culturing photosynthetic symbionts could be offered to the species.

Larger body size of Fis form (*G. fistulosa*) revealed by the total volume provides a first-order measure for the biomass. Assuming there was only subtle difference on the density of the soft tissue and calcitic skeleton between *T. sacculifer* (Normal and Sac-like forms) and Fis form (*G. fistulosa*), Fis form is estimated to be larger on its biomass. A trophic mode that different to *T. sacculifer* and buoyancy adjustment for water depth migration might be hypothesized to interpret the larger biomass. Larger organisms are also considered more successful on producing more gametes (Hemleben et al., 2012), which could be part of the survival strategy of Fis form (*G. fistulosa*).

4.4 Trophic mode of *G. fistulosa* (Fis form)

The previous result of shell $\delta^{13}C$ value of *G. fistulosa* (Chen, 2008) is following the positive $\delta^{13}C$-size relationship reported on extent spinose symbiotic species (Birch et al., 2013; Elderfield et al., 2002), and which implies the strong uptake of isotopically heavy metabolic carbon from the symbionts. Therefore, the species could be highly relied on symbiotic photosynthesis to attain energy, just like *T. sacculifer*. The generally larger surface

doi:10.6342/NTU202404142

area of *G. fistulosa* compared to *T. sacculifer* implies it might obtain more energy via its larger surface area and thus led to enhanced symbiotic photosynthesis. The extra energy produced could then become critical to its larger biomass (stemming from the evidence of total volume reported in this study). However, a more thorough analysis would be needed to understand the fractionation contribution of photosynthesis, metabolism and diet of the organism. Literally, *G. fistulosa* could be more sensitive to metabolism because of its improved respiration rate induced by larger surface area.

Apart from symbiotic photosynthesis, carnivorous food uptake might be available for *G. fistulosa* as *T. sacculifer.* By increasing its total volume, *G. fistulosa* would needs more amount of prey than *T. sacculifer* to maintain its body size (Signes et al., 1993). Moreover, assuming the prey palatability (which depends on optimum predator-prey length ratio) of *G. fistulosa* and *T. sacculifer* is following the modelled optimum (10:1 ratio)(Grigoratou et al., 2021), the former might be allowed to capture larger prey than *T. sacculifer*. *G. fistulosa* could be more specialist on diet compared to *T. sacculifer*, as its higher surface-to-volume ratio (combined with the surface area provided by spines in here) would improve the potential for food intake and thus it is not necessary for the organism to have a more generalist diet (Grigoratou et al., 2021). Besides, fluctuation on the prey abundance could also plays an important rule to the variation of the total volume.

4.5 Possible environmental controls for *G. fistulosa* (Fis form)

Based on the gross shell geochemical analyses carried in Chen (2008), *G. fistulosa* (Fis form) is considered lived in the part of the water column in between and partially

doi:10.6342/NTU202404142

overlapped with *T. sacculifer* and *N. dutertrei*. Since the geochemistry of the gross shell could be highly dominated by the lately produced chamber(s) as it occupied a huge part of the body, the deduced living depth/calcification depth (in between 80-100 m) might refer to more matured and adult stage of the species. Referring to the modern ocean condition in this part of the water column (80-100 m), salinity is almost reaching its maximum in the ocean (Appendix 3.3) and led to the increase of sea water density. Nitrate and phosphorate are higher in abundance than where *T. sacculifer* lived by following a gradually increasing trend (Appendix 3.1-3.2), which could be attributed to the settling of organic matters from the sea surface (Emerson et al., 2003). By combining the result of the vertical sea structure reconstruction prior and after the extinct of *G. fistulosa* (Fis form) (1.767-1.743 Ma) in Chen (2008), the sea water structure in the Solomon Sea is characterized with thinner mixed and shallower thermocline, which is consistent to the ENSO-like interpretation of Wara et al. (2005), as the difference found on reconstructed temperature (through Mg/Ca analysis) and $\delta^{18}O_{sw\ (SMOW)}$ between *G. fistulosa* (Fis form) *T. sacculifer* gradually decreases. Since the formation and expansion of Western Pacific Warm Pool (WPWP) would lead to increasing freshwater precipitation and therefore maintain stable mixed layer in the surface (de Boyer Montégut et al., 2007; Lukas and Lindstrom, 1991; Webster and Lukas, 1992). Thus, under the ancient ENSO-like condition, nutrients abundance and salinity might started ascend in shallower depth compared to the modern condition.

Some clues are sorted out here for the hydrodynamic strategy of *G. fistulosa*, as some hypothesized adaptive morphological traits are considered for the species to maintain balanced in deeper, denser part of the water column compared to *T. sacculifer*. Its shell density might be higher than *T. sacculifer* to increase settling speed, and which is also linked

doi:10.6342/NTU202404142

to the calcification effort (Caromel et al., 2014; Signes et al., 1993) of the species. Some physiological regulations toward the cytoplasm via incorporation of gas vesicles or adjustments to ionic concentration might also happened to lower the overall density of the organism (Kahn and Swift, 1978; Walsby et al., 1997). However, such mechanism would be difficult to be tested on fossils. Interestingly, presence of protuberance-bearing chamber and thus results in more irregular gross morphology and more spine beared, nevertheless, would counteracting the settling force provided by the hypothesized higher shell and overall density. Further simulation or experimental test would be necessary to understand exactly how the species is different from *T. sacculifer* on the hydrodynamics.

Because of the higher abundance of initial nutrients (phosphorate and nitrate) deduced for the depth matured *G. fistulosa* is considered lived. It is inevitable to assess the possible connection between the larger size of the species (than *T. sacculifer*) and raised nutrient abundance. The elevated nutrient concentration might be related to the settling and decompose of died planktons backed to dissolved ions from the upper part of the water column (Emerson et al., 2003) and thus provides critical prey resources for growth and symbiotic activities. As the prey abundance raises, larger final test size and more chambers would attained by the foraminifera (Takagi et al., 2018). This might be the reason why *G. fistulosa* is larger in size than *T. sacculifer*. Besides, size-normalised weights were found inversely related to both nitrate and phosphorate concentrations (Aldridge et al., 2012), implies that the calcification and therefore settling speed of *G. fistulosa* might be controlled by the nutrient level. However, temperature and carbonate ion concentrations could also involve in the calcification process (Bé et al., 1973; Russell et al., 2004; Schmidt et al., 2004;

doi:10.6342/NTU202404142

Spero et al., 1997; Spero et al., 1991), and further studies would be needed to determine which factor is more influential to the species.

doi:10.6342/NTU202404142

Chapter 5 Conclusion

G. fistulosa (Fis form) is showing larger total volume and surface area than *T. sacculifer* plexus (Normal and Sac-like forms). Moreover, *G. fistulosa* is smaller than *T. sacculifer* plexus on surface to total volume ratio (the S-V ratio). However, *G. fistulosa* is larger than *T. sacculifer* plexus on the S-V ratio under the same total volume. The larger total volume of *G. fistulosa* (Fis form) compared to *T. sacculifer* plexus (Normal and Sac-like forms) strengthens the hypothesis of *G. fistulosa* to be the late ontogenetic stage (s) of *T. sacculifer* (Chen, 2006). Besides, an environment-driven ecophenotype of *T. sacculifer* plexus could also be a possibility. By comparing with the previously reported data in Poole and Wade (2019), the more right-shifted regression fits of *G. fistulosa* compared to *T. sacculifer* plexus on the maximum length-surface area comparison is not observed in our 3D data (total volume-surface area comparison). The characteristic is argued by us as a bias, and could be attributed to 2D photography. Such bias could lead to wrong interpretation on the growth of *G. fistulosa* and *T. sacculifer* plexus, as they are highly similar on the total volume-surface area comparison.

G. fistulosa and *T. sacculifer* are sharing similar growth based on the regression analysis of the total volume-surface area comparison. Most individuals of *G. fistulosa* (Fis form) are register with strong variation on the surface area as total volume increases, which could be subjected to strong environmental control. Larger surface area found on *G. fistulosa* (Fis form) compared to *T. sacculifer* and its strong variation could be related to the general oxygen deficiency of oxygen level at the lower part of the water column. Moreover, the improved respiration rate attributed to the larger surface area could improve the relatively

doi:10.6342/NTU202404142

low metabolic activity and higher its contribution to the positive $\delta^{13}C$-size relationship reported in Chen (2008). The larger S-V ratio and therefore larger surface area on *G. fistulosa* (Fis form) than *T. sacculifer* under the same total volume could also be referred to enhanced symbiotic photosynthesis, as the surface area influences the abundance of symbionts on spinose planktonic foraminifers. Other than the gross morphology, the presence and number of the digitate protuberance could also be instrumental to provide additional surface area for more spine and improving respiration rate. Increased buoyancy and more space for culturing photosynthetic symbionts could be offered to the species. Larger total volume of *G. fistulosa* (Fis form) provides a first-order measure for the larger biomass, which could be attributed to a trophic mode that different from *T. sacculifer*. The ability to produce more gametes because of the larger body size could be part of the survival strategy of *G. fistulosa* (Fis form).

Under the ancient ENSO-like condition, nutrients abundance and salinity might started ascend in shallower depth compared to the modern condition. As *G.* fistulosa is considered to live in the deeper part of the water column compared to *T. sacculifer*, a different hydrodynamic strategy of *G. fistulosa* is proposed in this study with some hypothesized adaptive morphological traits are considered for the species to maintain balanced in the deeper depth.

doi:10.6342/NTU202404142

References

Aldridge, D., Beer, C., & Purdie, D. (2012). Calcification in the planktonic foraminifera Globigerina bulloides linked to phosphate concentrations in surface waters of the North Atlantic Ocean. *Biogeosciences*, *9*(5), 1725-1739.

Bé, Harrison, S. M., & Lott, L. (1973). Orbulina universa d'Orbigny in the Indian Ocean. *Micropaleontology*, *19*(2), 150-192.

Bé, A. (1980). Gametogenic calcification in a spinose planktonic foraminifer, Globigerinoides sacculifer (Brady). *Marine Micropaleontology*, *5*, 283-310.

Belanger, C. L. (2022). Volumetric analysis of benthic foraminifera: Intraspecific test size and growth patterns related to embryonic size and food resources. *Marine Micropaleontology*, *176*, 102170.

Berger, W. H. (1969). Kummerform foraminifera as clues to oceanic environments. *AAPG bulletin*, *53*(3), 706-706.

Bijma, J., Faber, W. W., & Hemleben, C. (1990). Temperature and salinity limits for growth and survival of some planktonic foraminifers in laboratory cultures. *Journal of foraminiferal research*, *20*(2), 95-116.

Bijma, J., & Hemleben, C. (1994). Population dynamics of the planktic foraminifer Globigerinoides sacculifer (Brady) from the central Red Sea. *Deep Sea Research Part I: Oceanographic Research Papers*, *41*(3), 485-510.

Birch, H., Coxall, H. K., Pearson, P. N., Kroon, D., & O'Regan, M. (2013). Planktonic foraminifera stable isotopes and water column structure: Disentangling ecological signals. *Marine Micropaleontology*, *101*, 127-145.

doi:10.6342/NTU202404142

Brady, H. B. (1877). II.—Supplementary note on the Foraminifera of the Chalk (?) of the New Britain Group. *Geological Magazine*, *4*(12), 534-536.

Brombacher, A., Searle-Barnes, A., Zhang, W., & Ezard, T. H. (2022). Analysing planktonic foraminiferal growth in three dimensions with foram3D: an R package for automated trait measurements from CT scans. *Journal of Micropalaeontology*, *41*(2), 149-164.

Brummer, G.-J. A., Hemleben, C., & Spindler, M. (1987). Ontogeny of extant spinose planktonic foraminifera (Globigerinidae): A concept exemplified byGlobigerinoides sacculifer (Brady) andG. Ruber (d'Orbigny). *Marine Micropaleontology*, *12*, 357-381.

Burke, J. E., Renema, W., Schiebel, R., & Hull, P. M. (2020). Three-dimensional analysis of inter-and intraspecific variation in ontogenetic growth trajectories of planktonic foraminifera. *Marine Micropaleontology*, *155*, 101794.

Caromel, A. G., Schmidt, D. N., Fletcher, I., & Rayfield, E. J. (2016). Morphological change during the ontogeny of the planktic foraminifera. *Journal of Micropalaeontology*, *35*(1), 2-19.

Caromel, A. G., Schmidt, D. N., Phillips, J. C., & Rayfield, E. J. (2014). Hydrodynamic constraints on the evolution and ecology of planktic foraminifera. *Marine Micropaleontology*, *106*, 69-78.

Chen, C.-Y. (2006). *Exploring the Extinction of Globigerinoides fistulosus from the Perspective of 'Heterochrony'* [Unpublished Master's Thesis]National Taiwan University.

doi:10.6342/NTU202404142

Chen, C.-Y. (2008). *A study on the disappearance of Globigerinoides fistulosus and its relationship to the hydrological change of the tropical pacific* [Unpublished Undergraduate's Thesis] National Taiwan University.

Chen, W.-L., Kang, J.-C., Kimoto, K., Song, Y.-F., Yin, G.-C., Swisher, R. E., Lu, C.-H., Kuo, L.-W., Huang, J.-J. S., & Lo, L. (2023). μ-Computed tomographic data of fossil planktonic foraminifera from the western Pacific Ocean: a dataset concerning two biostratigraphic events during the Early Pleistocene. *Frontiers in Ecology and Evolution*, *11*, 1171891.

Chuang, C.-K., Lo, L., Zeeden, C., Chou, Y.-M., Wei, K.-Y., Shen, C.-C., Mii, H.-S., Chang, Y.-P., & Tung, Y.-H. (2018). Integrated stratigraphy of ODP Site 1115 (Solomon Sea, southwestern equatorial Pacific) over the past 3.2 Ma. *Marine Micropaleontology*, *144*, 25-37.

d'Orbigny, A. D. (1846). *Foraminifères fossiles du bassin tertiaire de Vienne (Autriche): découverts par Joseph de Hauer*. McLean Paleontological Laboratory.

de Boyer Montégut, C., Mignot, J., Lazar, A., & Cravatte, S. (2007). Control of salinity on the mixed layer depth in the world ocean: 1. General description. *Journal of Geophysical Research: Oceans*, *112*(C6).

Depuydt, P., Barras, C., Toucanne, S., Fossile, E., & Mojtahid, M. (2023). Implication of size fraction on benthic foraminiferal-based paleo-reconstructions: A case study from the Bay of Biscay (NE Atlantic). *Marine Micropaleontology*, *181*, 102242.

Duan, B., Li, T., & Pearson, P. N. (2021). Three dimensional analysis of ontogenetic variation in fossil globorotaliiform planktic foraminiferal tests and its implications

doi:10.6342/NTU202404142

for ecology, life processes and functional morphology. *Marine Micropaleontology*, *165*, 101989.

Elderfield, H., Vautravers, M., & Cooper, M. (2002). The relationship between shell size and Mg/Ca, Sr/Ca, δ18O, and δ13C of species of planktonic foraminifera. *Geochemistry, Geophysics, Geosystems*, *3*(8), 1-13.

Emerson, S., Hedges, J., & Heinrich, D. (2003). Sediment Diagenesis and benthic flux, treatise on geochemistry. In: Elsevier: Amsterdam.

Görög, Á., Szinger, B., Tóth, E., & Viszkok, J. (2012). Methodology of the micro-computer tomography on foraminifera. *Palaeontologia Electronica*, *15*(1), 15.

Grigoratou, M., Monteiro, F. M., Ridgwell, A., & Schmidt, D. N. (2021). Investigating the benefits and costs of spines and diet on planktonic foraminifera distribution with a trait-based ecosystem model. *Marine Micropaleontology*, *166*, 102004.

Hammer, Ø., & Harper, D. A. (2001). Past: paleontological statistics software package for educaton and data anlysis. *Palaeontologia Electronica*, *4*(1), 1.

Hay, W. W., & Sandberg, P. A. (1967). The scanning electron microscope, a major break-through for micropaleontology. *Micropaleontology*, 407-418.

Hemleben, C., Spindler, M., & Anderson, O. R. (2012). *Modern planktonic foraminifera*. Springer Science & Business Media.

Hemleben, C., Spindler, M., Breitinger, I., & Ott, R. (1987). Morphological and physiological responses ofGlobigerinoides sacculifer (Brady) under varying laboratory conditions. *Marine Micropaleontology*, *12*, 305-324.

Hori, M., Shirai, K., Kimoto, K., Kurasawa, A., Takagi, H., Ishida, A., Takahata, N., & Sano, Y. (2018). Chamber formation and trace element distribution in the calcite walls of

doi:10.6342/NTU202404142

laboratory cultured planktonic foraminifera (Globigerina bulloides and Globigerinoides ruber). *Marine Micropaleontology*, *140*, 46-55.

Iwasaki, S., Kimoto, K., Sasaki, O., Kano, H., & Uchida, H. (2019). Sensitivity of planktic foraminiferal test bulk density to ocean acidification. *Scientific reports*, *9*(1), 9803.

Kahn, N., & Swift, E. (1978). Positive buoyancy through ionic control in the nonmotile marine dinoflagellate Pyrocystis noctiluca Murray ex Schuett 1. *Limnology and Oceanography*, *23*(4), 649-658.

LeRoy, L. W. (1939). Some small foraminifera, ostracode and otoliths from the Neogene (“Miocene”) of the Rokan‐Tapanoeli area, Central Sumatra. *Natuurkundig Tijdschrift voor Nederlandsch‐Indië*, *99*, 215.

Lisiecki, L. E., & Raymo, M. E. (2005). A Pliocene‐Pleistocene stack of 57 globally distributed benthic δ18O records. *Paleoceanography*, *20*(1).

Lukas, R., & Lindstrom, E. (1991). The mixed layer of the western equatorial Pacific Ocean. *Journal of Geophysical Research: Oceans*, *96*(S01), 3343-3357.

Olsson, R. (1972). Growth changes in the Globorotalia fohsi lineage. *Eclogae Geologicae Helvetiae*, *65*(1), 165-184.

Olsson, R. K. (1973). What is a kummerform planktonic foraminifer? *Journal of Paleontology*, 327-329.

OriginLab Corporation, N., MA, USA. (Version 2021). *Origin(Pro)*. In

Poole, C. R., & Wade, B. S. (2019). Systematic taxonomy of the Trilobatus sacculifer plexus and descendant Globigerinoidesella fistulosa (planktonic foraminifera). *Journal of Systematic Palaeontology*, *17*(23), 1989-2030.

doi:10.6342/NTU202404142

Reuss, A. v. (1850). Neues Foraminiferen aus den schicten des Osterreichischen Tertiarbeckens. *Denkschriften der Akademie des Wissenschaften Wein*, *1*, 365-390.

Russell, A. D., Hönisch, B., Spero, H. J., & Lea, D. W. (2004). Effects of seawater carbonate ion concentration and temperature on shell U, Mg, and Sr in cultured planktonic foraminifera. *Geochimica et Cosmochimica Acta*, *68*(21), 4347-4361.

Schlitzer, R. (2023). *Ocean Data View*. odv.awi.de

Schmidt, D. N., Renaud, S., Bollmann, J., Schiebel, R., & Thierstein, H. R. (2004). Size distribution of Holocene planktic foraminifer assemblages: biogeography, ecology and adaptation. *Marine Micropaleontology*, *50*(3-4), 319-338.

Schubert, R. J. (1910). Ueber Foraminiferen und einen Fischotolithen aus dem fossilen Globigerinenschlamm von Neu-Guinea. *Verhandlungen der Geologischen Reichsanstalt, Wien*, *1910*, 318-328.

Signes, M., Bijma, J., Hemleben, C., & Ott, R. (1993). A model for planktic foraminiferal shell growth. *Paleobiology*, *19*(1), 71-91.

Spero, H. J., Bijma, J., Lea, D. W., & Bemis, B. E. (1997). Effect of seawater carbonate concentration on foraminiferal carbon and oxygen isotopes. *Nature*, *390*(6659), 497-500.

Spero, H. J., Lerche, I., & Williams, D. F. (1991). Opening the carbon isotope" vital effect" black box, 2, Quantitative model for interpreting foraminiferal carbon isotope data. *Paleoceanography*, *6*(6), 639-655.

doi:10.6342/NTU202404142

Spezzaferri, S., Kucera, M., Pearson, P. N., Wade, B. S., Rappo, S., Poole, C. R., Morard, R., & Stalder, C. (2015). Fossil and genetic evidence for the polyphyletic nature of the planktonic foraminifera" Globigerinoides", and description of the new genus Trilobatus. *PloS one*, *10*(5), e0128108.

Takagi, H., Kimoto, K., Fujiki, T., & Moriya, K. (2018). Effect of nutritional condition on photosymbiotic consortium of cultured Globigerinoides sacculifer (Rhizaria, Foraminifera). *Symbiosis*, *76*, 25-39.

Takahashi, K., Cortese, G., Frost, G. M., Gerbaudo, S., Goodliffe, A. M., Ishikawa, N., Lackschewitz, K. S., Perembo, R. C., Resig, J. M., & Siesser, W. G. (2001). 4. Summary of revised age assignments for ODP Leg 180. *In: Huchon, P., Taylor, B., Klaus, A.(Eds.), Proceedings ODP, Scientific Results [Online]. Available from World Wide Web:{http://www-odp. tamu. edu/publications/180_SR/152/152. htm}*, *180*.

Taylor, B., Huchon, , P., K., A.,, & al., e. (1999). Chapter 9: Site 1115. *Proceedings of the Ocean Drilling Program, Init. Reports 180*, *180*, 1-226.

Vanadzina, K., & Schmidt, D. N. (2022). Developmental change during a speciation event: evidence from planktic foraminifera. *Paleobiology*, *48*(1), 120-136.

Wade, B. S., Pearson, P. N., Berggren, W. A., & Pälike, H. (2011). Review and revision of Cenozoic tropical planktonic foraminiferal biostratigraphy and calibration to the geomagnetic polarity and astronomical time scale. *Earth-Science Reviews*, *104*(1-3), 111-142.

Walsby, A. E., Hayes, P. K., Boje, R., & Stal, L. J. (1997). The selective advantage of buoyancy provided by gas vesicles for planktonic cyanobacteria in the Baltic Sea. *The New Phytologist*, *136*(3), 407-417.

doi:10.6342/NTU202404142

Wara, M. W., Ravelo, A. C., & Delaney, M. L. (2005). Permanent El Niño-like conditions during the Pliocene warm period. *Science*, *309*(5735), 758-761.

Webster, P. J., & Lukas, R. (1992). TOGA COARE: The coupled ocean–atmosphere response experiment. *Bulletin of the American Meteorological Society*, *73*(9), 1377-1416.

Wei, K.-Y. (1987). Multivariate morphometric differentiation of chronospecies in the late Neogene planktonic foraminiferal lineageGloboconella. *Marine Micropaleontology*, *12*, 183-202.

doi:10.6342/NTU202404142

Appendix 1 Result of two-sample t test for equal means

H0: $\mu 1 = \mu 2$

H1: $\mu 1 \neq \mu 2$

How to interpret:

E.g.,

t-value : 8.8905 p-value (same mean): 6.2976E-15

Critical t-value (p=0.05): 1.9794

Uneq. Var. t-value : 9.0086 p-value (same mean): 1.7001E-14

If p-value < α=0.05 ----------> significantly different

If p-value > α=0.05 ----------> no significant difference

Parameters analyzed:

V: Total volume

S: Surface area

SV: Surface area to total volume ratio

E.g., V_Fis = total volume of the Fis form

doi:10.6342/NTU202404142

1.1 Result of V_Fis vs. V_Normal

V_Fis		V_Normal	
N:	64	N:	61
Mean:	9.4964E07	Mean:	4.2895E07
95% conf.:	(8.4869E07 1.0506E08)	95% conf.:	(3.7278E07 4.8512E07)
Variance:	1.6335E15	Variance:	4.8097E14

Difference between means: 5.2069E07

95% conf. interval (parametric): (4.0476E07 6.3662E07)

95% conf. interval (bootstrap): (4.0979E07 6.3218E07)

t-value :	8.8905	p-value (same mean):	6.2976E-15
Critical t-value (p=0.05):	1.9794		
Uneq. Var. t -value :	9.0086	p-value (same mean):	1.7001E-14
Monte Carlo permutation:		p-value (same mean):	0.0001

Result: Significant different

---

doi:10.6342/NTU202404142

1.2 Result of V_Fis vs. V_Sac-like

V_Fis		V_Sac-like	
N:	64	N:	41
Mean:	9.4964E07	Mean:	4.7308E07
95% conf.:	(8.4869E07 1.0506E08)	95% conf.:	(3.8996E07 5.562E07)
Variance:	1.6335E15	Variance:	6.9352E14

Difference between means: 4.7656E07

95% conf. interval (parametric): (3.3527E07 6.1786E07)

95% conf. interval (bootstrap): (3.4732E07 6.0099E07)

t-value :	6.6892	p-value (same mean):	1.1913E-09
Critical t-value (p=0.05):	1.9833		
Uneq. Var. t-value :	7.3155.	p-value (same mean):	5.7813E-11
Monte Carlo permutation:		p-value (same mean):	0.0001

Result: Significantly different

---

doi:10.6342/NTU202404142

1.3 Result of V_Normal vs. V_Sac-like

V_Normal		V_Sac-like	
N:	61	N:	41
Mean:	4.2895E07	Mean:	4.7308E07
95% conf.:	(3.7278E07 4.8512E07)	95% conf.:	(3.8996E07 5.562E07)
Variance:	4.8097E14	Variance:	6.9352E14

Difference between means: 4.4128E06

95% conf. interval (parametric): (-5.1192E06 1.3945E07)

95% conf. interval (bootstrap): (-5.1082E06 1.3797E07)

t-value :	0.91848.	p-value (same mean):	0.36058
Critical t-value (p=0.05):	1.984		
Uneq. var. t-value :	0.88612	p-value (same mean):	0.37838
Monte Carlo permutation:		p-value (same mean):	0.359

Result: Not significant difference

---

doi:10.6342/NTU202404142

1.4 Result of S_Fis vs. S_Normal

S_Fis		S_Normal	
N:	53	N:	61
Mean:	1.7675E06	Mean:	6.91E05
95% conf.:	(9.872E05 2.5477E06)	95% conf.:	(6.2386E05 7.5814E05)
Variance:	9.4403E12	Variance:	6.8719E10

Difference between means:	1.0765E06
95% conf. interval (parametric):	(2.948E05 1.8581E06)
95% conf. interval (bootstrap):	(2.3446E05 1.5598E06)

t -value:	2.7264	p-value (same mean):	0.0073539
Critical t value (p=0.05):	1.9798		
Uneq. Var. t-value :	2.7485	p-value (same mean):	0.0078336
Monte Carlo permutation:		p-value (same mean):	0.0001

Result: Significantly different

---

doi:10.6342/NTU202404142

1.5 Result of S_Fis vs. S_Sac-like

S_Fis		S_Sac-like	
N:	53	N:	41
Mean:	1.7675E06	Mean:	7.5418E05
95% conf.:	(9.872E05 2.5477E06)	95% conf.:	(6.574E05 8.5097E05)
Variance:	9.4403E12	Variance:	9.4026E10

Difference between means: 1.0133E06

95% conf. interval (parametric): (56699 1.9699E06)

95% conf. interval (bootstrap): (1.6418E05 1.5083E06)

t-value :	2.1013	p-value (same mean):	0.038102
Critical t-value (p=0.05):	1.9837		
Uneq. Var. t-value :	2.5774	p-value (same mean):	0.012312
Monte Carlo permutation:		p-value (same mean):	0.0001

Result: Significantly different

---

doi:10.6342/NTU202404142

1.6 Result of S_Normal vs. S_Sac-like

S_Normal		S_Sac	
N:	61	N:	41
Mean:	6.91E05	Mean:	7.5418E05
95% conf.:	(6.2386E05 7.5814E05)	95% conf.:	(6.574E05 8.5097E05)
Variance:	6.8719E10	Variance:	9.4026E10

Difference between means: 63181

95% conf. interval (parametric): (-49320 1.7568E05)

95% conf. interval (bootstrap): (-52032 1.7881E05)

t-value :	1.1142	p-value (same mean):	0.26786
Critical t-value (p=0.05):	1.984		
Uneq. var. t-value :	1.0804	p-value (same mean):	0.28336
Monte Carlo permutation:		p-value (same mean):	0.2662

Result: Not significantly different

---

doi:10.6342/NTU202404142

1.7 Result of SV_Fis vs. SV_Normal

SV_Fis		SV_Normal	
N:	53	N:	61
Mean:	0.015384	Mean:	0.017678
95% conf.:	(0.014805 0.015963)	95% conf.:	(0.01684 0.018516)
Variance:	5.1968E-06	Variance:	1.0705E-05

Difference between means: 0.0022946

95% conf. interval (parametric): (0.0012893 0.0032999)

95% conf. interval (bootstrap): (0.0012776 0.0032464)

t-value :	4.5188	p-value (same mean):	1.4577E-05
Critical t-value (p=0.05):	1.9798		
Uneq. var. t-value :	4.506	p-value (same mean):	1.6939E-05
Monte Carlo permutation:		p-value (same mean):	0.0001

Result: Significantly different

---

doi:10.6342/NTU202404142

1.8 Result of SV_Fis vs. SV_Sac-like

SV_Fis		SV_Sac-like	
N:	53	N:	41
Mean:	0.015384	Mean:	0.017573
95% conf.:	(0.014805 0.015963)	95% conf.:	(0.016546 0.0186)
Variance:	5.1968E-06	Variance:	1.0583E-05

Difference between means: 0.0021893

95% conf. interval (parametric): (0.0011082 0.0032704)

95% conf. interval (bootstrap): (0.0010523 0.0033031)

t-value :	4.0173	p-value (same mean):	0.00011343
Critical t-value (p=0.05):	1.9837		
Uneq. Var. t-value :	3.744	p-value (same mean):	0.00038362
Monte Carlo permutation:		p-value (same mean):	0.0002

Result: Significantly different

---

doi:10.6342/NTU202404142

1.9 Result of SV_Normal vs. SV_Sac-like

SV_Normal		SV_Sac	
N:	62	N:	41
Mean:	0.017589	Mean:	0.017573
95% conf.:	(0.016745 0.018432)	95% conf.:	(0.016546 0.0186)
Variance:	1.1026E-05	Variance:	1.0583E-05

Difference between means: 1.5747E-05

95% conf. interval (parametric): (-0.0012996 0.0013311)

95% conf. interval (bootstrap): (-0.0012324 0.0013061)

t-value : 0.023749 p-value (same mean): 0.9811

Critical t-value (p=0.05):1.9837

Uneq. Var. t-value : 0.02385 p-value (same mean): 0.98103

Monte Carlo permutation: p-value (same mean): 0.9827

Result: Not significantly different

---

doi:10.6342/NTU202404142

Appendix 2 Descriptive statistics of total volume, surface area and Surface area to total volume (S-V) ratio

2.1 Table for descriptive statistical comparison of the total volume of Fis, Normal and Sac-like forms.

	G. fistulosa (Fis form)	*T. sacculifer* (Normal form)	*T. sacculifer* (Sac-like form)
Mean	9.95×10^{7} μm³	4.29×10^{7} μm³	4.73×10^{7} μm³
Standard error	5.74×10^{6} μm³	2.81×10^{6} μm³	4.11×10^{6} μm³
Median	9.40×10^{7} μm³	4.21×10^{7} μm³	4.50×10^{7} μm³
Standard deviation	4.18×10^{7} μm³	2.19×10^{7} μm³	2.63×10^{7} μm³
Sample variance	1.75×10^{15} μm³	4.81×10^{14} μm³	6.94×10^{14} μm³
Kurtosis	-0.18	-1.40	-0.16
Skewness	4.00×10^{-1}	1.09×10^{-1}	6.60×10^{-1}
Range	1.66×10^{8} μm³	7.00×10^{7} μm³	9.83×10^{7} μm³
Minimum	3.04×10^{7} μm³	1.16×10^{7} μm³	1.42×10^{7} μm³
Maximum	1.96×10^{8} μm³	8.16×10^{7} μm³	1.12×10^{8} μm³
Sample numbers	53	61	41

doi:10.6342/NTU202404142

2.2 Table for descriptive statistical comparison of the surface area of Fis, Normal and Sac-like forms.

	G. fistulosa (Fis form)	*T. sacculifer* (Normal form)	*T. sacculifer* (Sac-like form)
Mean	$1.45x10^{6}$ μm²	$6.91x10^{5}$ μm²	$7.54x10^{5}$ μm²
Standard error	$6.69x10^{4}$ μm²	$3.36x10^{4}$ μm²	$4.7,9x10^{4}$ μm²
Median	$1.45x10^{6}$ μm²	$7.00x10^{5}$ μm²	$7.59x10^{5}$ μm²
Standard deviation	$4.87x10^{6}$ μm²	$2.62x10^{5}$ μm²	$3.07x10^{5}$ μm²
Variance	$2.38x10^{11}$ μm²	$6.87x10^{10}$ μm²	$9.40x10^{10}$ μm²
Kurtosis	$5.26x10^{-1}$	-1.423	$-4.82x10^{-1}$
Skewness	$6.61x10^{-1}$	$-5.98x10^{-2}$	$4.10x10^{-1}$
Range	$2.24x10^{6}$ μm²	$8.15x10^{5}$ μm²	$1.13x10^{6}$ μm²
Minimum	$6.12x10^{5}$ μm²	$2.82x10^{5}$ μm²	$3.33x10^{5}$ μm²
Maximum	$2.85x10^{6}$ μm²	$1.097x10^{6}$ μm²	$1.46x10^{6}$ μm²
Sample numbers	62	61	41

doi:10.6342/NTU202404142

2.3 Table for descriptive statistical comparison of the S-V ratio of Fis, Normal and Sac-like forms.

	G. fistulosa (Fis form)	*T. sacculifer* (Normal form)	*T. sacculifer* (Sac-like form)
Mean	$1.53x10^{-2}$ μm^{-1}	$1.77x10^{-2}$ μm^{-1}	$1.76x10^{-2}$ μm^{-1}
Standard error	$3.15x10^{-4}$ μm^{-1}	$4.19x10^{-4}$ μm^{-1}	$5.08x10^{-4}$ μm^{-1}
Median	$1.51x10^{-2}$ μm^{-1}	$1.65x10^{-2}$ μm^{-1}	$1.69x10^{-2}$ μm^{-1}
Standard deviation	$2.30x10^{-3}$ μm^{-1}	$3.27x10^{-3}$ μm^{-1}	$3.25x10^{-3}$ μm^{-1}
Variance	$5.27x10^{-6}$ μm^{-1}	$1.07x10^{-5}$ μm^{-1}	$1.06x10^{-5}$ μm^{-1}
Kurtosis	$-3.30x10^{-1}$	-1.01	$-8.85x10^{-1}$
Skewness	$6.66x10^{-1}$	$5.68x10^{-1}$	$5.65x10^{-1}$
Range	$8.69x10^{-3}$ μm^{-1}	$1.12x10^{-2}$ μm^{-1}	$1.05x10^{-2}$ μm^{-1}
Minimum	$1.2x10^{-2}$ μm^{-1}	$1.32x10^{-2}$ μm^{-1}	$1.30x10^{-2}$ μm^{-1}
Maximum	$2.10x10^{-2}$ μm^{-1}	$2.44x10^{-2}$ μm^{-1}	$2.35x10^{-2}$ μm^{-1}
Sample numbers	62	61	41

doi:10.6342/NTU202404142

Appendix 3 Bathymetric profile of nutrients and salinity

3.1 Bathymetric profile of nitrate

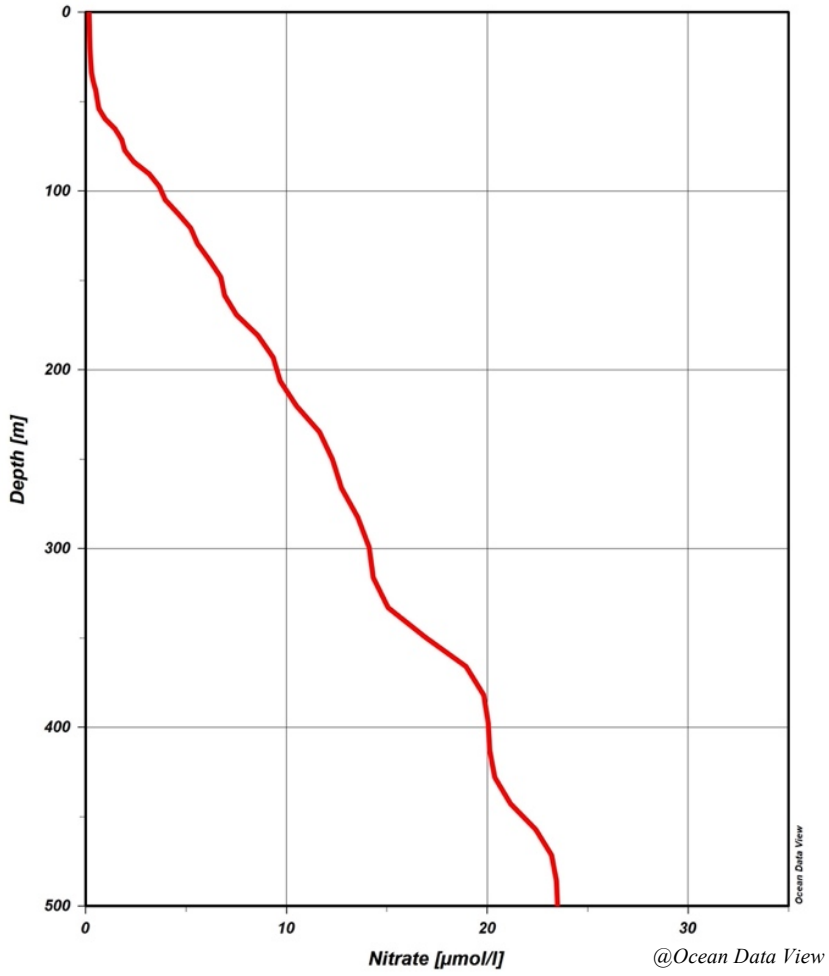

A gradually increased curve is found as the depth increases. Depth = 500.

doi:10.6342/NTU202404142

3.2 Bathymetric profile of phosphate

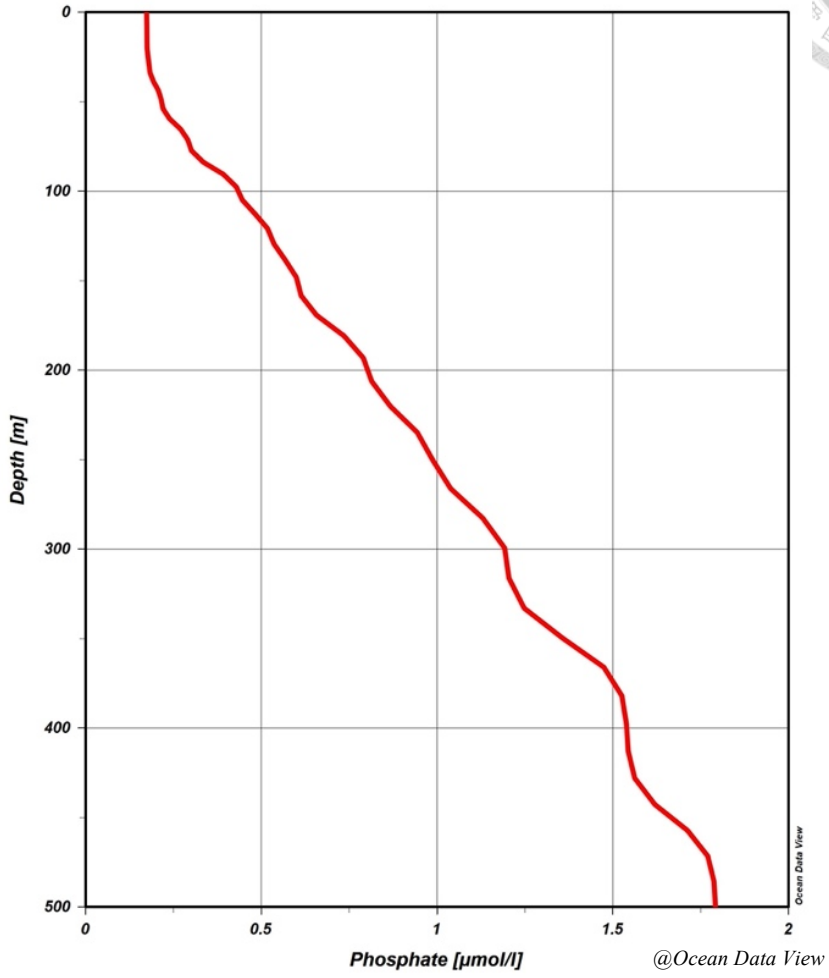

A gradually increased curve is found as the depth increases. Depth = 500 m.

doi:10.6342/NTU202404142

3.3 Bathymetric profile of salinity

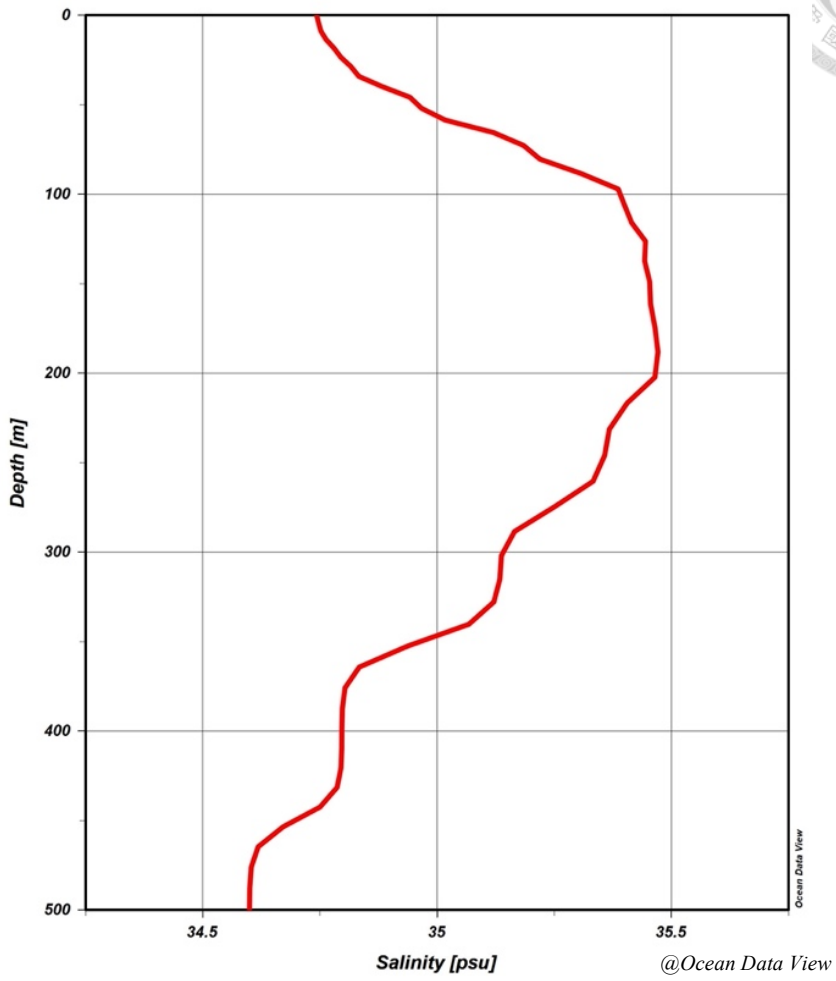

A rapidly increased curve is found as the depth increases until reaching the peak at 35 psu at around 200 m in depth. Below the peak, the salinity gradually decreases. Depth = 500 m

doi:10.6342/NTU202404142